This is a preprint, the final version is subject to change, of the American Mineralogist (MSA)
Cite as Authors (Year) Title. American Mineralogist, in press.
(DOI will not work until issue is live.) DOI: http://dx.doi.org/10.2138/am-2017-5770

Revision 2

Equation of State and Hyperfine Parameters of High-Spin Bridgmanite in the Earth's Lower Mantle by Synchrotron X-Ray Diffraction and Mössbauer Spectroscopy

Zhu Mao[1*], Fan Wang[1], Jung-Fu Lin[2,3*], Suyu Fu[1,2], Jing Yang[2], Xiang Wu[4], Takuo Okuchi[5], Naotaka Tomioka[6], Vitali B. Prakapenka[7], Yuming Xiao[8], Paul Chow[8]

[1]Laboratory of Seismology and Physics of Earth's Interior, School of Earth and Planetary Sciences, University of Science and Technology of China, Hefei, Anhui 230026, China

[2]Department of Geological Sciences, Jackson School of Geosciences, The University of Texas at Austin, Austin, TX 78712, USA

[3]Center for High Pressure Science and Technology Advanced Research (HPSTAR), Shanghai 130012, China

[4]State Key Laboratory of Geological Processes and Mineral Resources, China University of Geosciences, Wuhan 430074, China

[5]Institute for Study of the Earth's Interior, Okayama University, Misasa, Tottori 682-0193, Japan

[6]Kochi Institute for Core Sample Research, Japan Agency for Marine-Earth Science and Technology, Nankoku, Kochi 783-8502, Japan

[7]Center for Advanced Radiation Sources, University of Chicago, Chicago, IL 60637, USA

Corresponding author: zhumao@ustc.edu.cn, afu@jsg.utexas.edu

[8]HPCAT, Geophysical Laboratory, Carnegie Institution of Washington, Argonne, IL 60439, USA

Abstract

In this study, we performed synchrotron X-ray diffraction (XRD) and Mössbauer spectroscopy (SMS) measurements on two single-crystal bridgmanite samples ($Mg_{0.94}Fe_{0.04}^{2+}Fe_{0.02}^{3+}Al_{0.01}Si_{0.99}O_3$ (Bm6) and $Mg_{0.89}Fe_{0.024}^{2+}Fe_{0.096}^{3+}Al_{0.11}Si_{0.89}O_3$ (Al-Bm11)) to investigate the combined effect of Fe and Al on the hyperfine parameters, lattice parameters, and equation of state (EoS) of bridgmanite up to 130 GPa. Our SMS results show that Fe^{2+} and Fe^{3+} in Bm6 and Al-Bm11 are predominantly located in the large pseudo-dodecahedral sites (A-site) at lower-mantle pressures. The observed drastic increase in the hyperfine quadrupole splitting (QS) between 13 and 32 GPa can be associated with an enhanced local distortion of the A-site Fe^{2+} in Bm6. In contrast to Bm6, the enhanced lattice distortion and the presence of extremely high QS values of Fe^{2+} are not observed in Al-Bm11 at high pressures. Our results here support the notion that the occurrence of the extremely high QS component of approximately 4 mm/s in bridgmanite is due to the lattice distortion in the high-spin (HS) A-site Fe^{2+}, instead of the occurrence of the intermediate-spin state. Both A-site Fe^{2+} and Fe^{3+} in Bm6 and Al-Bm11 remain in the HS state at lower-mantle pressures. Together with XRD results, we present the first experimental evidence that the enhanced lattice distortion of A-site Fe^{2+} does not cause any detectable variation in the EoS parameters, but is associated with anomalous variations in the bond length,

tilting angle, and shear strain in the octahedra of Bm6. Analysis of the obtained EoS parameters of bridgmanite at lower-mantle pressures indicates that the substitution of Fe in bridgmanite will cause an enhanced density and a reduced bulk sound velocity (V_Φ), whereas the Al and Fe substitution has a reduced effect on density and a negligible effect on V_Φ. These experimental results provide new insight into the correlation between lattice, hyperfine, and EoS parameters of bridgmanite in the Earth's lower mantle.

Key words: bridgmanite, lattice distortion, equation of state, Fe and Al, lower mantle, high-spin

Introduction

Bridgmanite, $(Mg,Fe)(Fe,Al,Si)O_3$, is the most abundant mineral in the Earth's lower mantle occupying approximately 75% by volume in a pyrolitic mantle composition or as high as ~93% in the chondritic Earth model with a Si-enriched lower mantle (Hirose 2002; Irifune et al. 2010; Murakami et al. 2012; Ringwood 1975). In the past few decades, physical properties of bridgmanite at relevant pressure and temperature (P-T) conditions of the lower mantle have attracted extensive research interest (e.g. Hemley and Cohen 1992; McCammon 1997; Stixrude and Cohen 1993; Tsuchiya et al. 2004). In particular, recent experimental and theoretical studies have reported that Fe in lower-mantle bridgmanite undergoes spin pairing transitions, calling for investigations into the effect of Fe spin transition on the physical properties of

bridgmanite at lower-mantle pressures (e.g. Catalli et al. 2011; Catalli et al. 2010; Goncharov et al. 2010; Hsu et al. 2012; Lin et al. 2008; Lin et al. 2012; Mao et al. 2011; Mao et al. 2015; McCammon et al. 2008; Tsuchiya and Wang 2013). However, the spin and valence states of iron in bridgmanite remain controversial (e.g. see Lin et al. 2013 for a review).

Fe can exist as both Fe^{2+} and Fe^{3+} in lower-mantle bridgmanite in large pseudo-dodecahedral sites (A-site) and small octahedral sites (B-site) (Lin et al. 2013), complicating our understanding of the spin states of Fe in bridgmanite. Thus far, both experimental and theoretical studies are in agreement that Fe^{3+} in the B-site will undergo the high-spin (HS) to low-spin (LS) transition at lower-mantle pressures, but the A-site Fe^{3+} will stay in the HS state (Bengtson et al. 2009b; Catalli et al. 2011; Catalli et al. 2010; Dorfman et al. 2015; Fujino et al. 2014; Fujino et al. 2012; Hsu et al. 2011; Hsu et al. 2012; Lin et al. 2013; Lin et al. 2016). Although Fe^{2+} will only locate at the A-site in bridgmanite, the spin state of Fe^{2+} is still under debate (Bengtson et al. 2009b; Hsu et al. 2010; Hsu and Wentzcovitch 2014; Jackson et al. 2005; Li et al. 2006; Lin et al. 2012; McCammon et al. 2010; McCammon et al. 2008; Shukla et al. 2015). High-pressure Mössbauer spectroscopy studies have shown that the quadrupole splitting (QS) of the A-site Fe^{2+} increases drastically to an extremely high value of ~4 mm/s at approximately 18-30 GPa (Lin et al. 2012; Lin et al. 2013; Mao et al. 2011; McCammon et al. 2010; McCammon et al. 2008; Narygina et al. 2010). The anomalous increase in the QS of A-site Fe^{2+} in bridgmanite has been interpreted

as the HS to intermediate-spin (IS) transition by high-pressure Mössbauer studies, which has been proposed to produce a softening in the spontaneous shear strain and affect the octahedral tilting during compression (Boffa Ballaran et al. 2012; Lin et al. 2008; McCammon et al. 2010; McCammon et al. 2008; Narygina et al. 2010). However, theoretical calculations have pointed out that the IS Fe^{2+} in bridgmanite is energetically disfavored and highly unlikely to be stable at lower-mantle pressures, and the observed extremely high QS component is caused by the enhanced lattice distortion of the HS Fe^{2+} in the A-site (Bengtson et al. 2009a; Hsu et al. 2010; Hsu and Wentzcovitch 2014).

The influence of the spin states of Fe^{3+} and Fe^{2+} on the physical properties, in particular the equation of state (EoS), of bridgmanite is a crucial issue to understand the chemistry and dynamics of the lower-mantle. Theoretical and experimental studies have shown that the spin transition of B-site Fe^{3+} in bridgmanite can cause an abrupt reduction in its unit cell volume and softening in its bulk modulus at high pressure (Catalli et al. 2011; Hsu et al. 2011; Tsuchiya and Wang 2013). A Recent experimental study has observed an anomalous collapse in the volume of bridgmanite with 10% Fe between 18 and 25 GPa at 300 K (Mao et al. 2015). The cause for the observed anomalous change in the volume of bridgmanite remains unclear because the spin transition of B-site Fe^{3+} occurs coincidently with the enhanced lattice distortion of A-site Fe^{2+} and we still lack of direct experimental evidence for the effect of enhanced lattice distortion of A-site Fe^{2+} on the EoS parameters of bridgmanite (Mao et al.,

111 2015). In addition, most previous high-pressure studies for the EoS of bridgmanite did
112 not determine the spin and valence states of Fe in the powder samples at high pressures,
113 complicating our understanding of the effects of different spin and valence states of
114 Fe on the EoS of bridgmanite (Andrault et al. 2001; Boffa Ballaran et al. 2012;
115 Dorfman et al. 2013; Lundin et al. 2008; Mao et al. 1991; Nishio-Hamane et al. 2008).
116
117 Besides Fe, lower-mantle bridgmanite is expected to accommodate ~10% Al via the
118 coupled substitution of Fe^{3+}-Al^{3+} and/or Al^{3+}-Al^{3+} to replace Mg^{2+} in the pseudo-
119 dodecahedral A site and the octahedral B-site Si^{4+} (Frost et al. 2004; Irifune et al. 1996;
120 Irifune et al. 2010; McCammon 1997; Vanpeteghem et al. 2006). The Fe^{2+}, Fe^{3+}, and
121 Al^{3+} contents in bridgmanite in a pyrolitic composition have been reported to change
122 with depth in the lower mantle (e.g., Irifune et al. 2010). Theoretical calculations have
123 shown that the addition of Al does not affect the response of the A-site Fe^{3+} spin states
124 to pressure (Hsu et al. 2012), yet how the presence of Al may influence the lattice
125 distortion of A-site Fe^{2+} is unknown. In addition, although previous experimental
126 studies have yielded a wealth of results on the effects of Fe and Al on the EoS
127 parameters of bridgmanite using X-ray diffraction (XRD) in a diamond anvil cell
128 (DAC), the spin states of Fe in (Fe,Al)-bearing bridgmanite are mostly not determined
129 in these studies, and the experimental results on the combined effects of Fe and Al on
130 the EoS parameters of bridgmanite are still controversial (Andrault et al. 2001; Boffa
131 Ballaran et al. 2012; Dorfman et al. 2012; Glazyrin et al. 2014; Nishio-Hamane et al.
132 2008). For example, Andrault et al. (2001) showed that the presence of Fe and Al can

133 increase the isothermal bulk modulus at ambient conditions, K_{0T}, by 4% relative to
134 that of $MgSiO_3$-bridgmanite (Mg-Bm) if the initial pressure derivative of the
135 isothermal bulk modulus is fixed to the value of 4. In contrast, two other studies have
136 shown that the presence of 11-13% Fe and 12-15% Al leads to a 3-4% reduction in K_0
137 with a fixed K_0'=4 using Mg-Bm as the reference (Catalli et al. 2011; Nishio-Hamane
138 et al. 2008). As a result, the effects of the Al and Fe chemistry variation and iron
139 valence and spin state on the derived EoS parameters of these bridgmanite samples
140 remain poorly understood.
141
142 To correlate the lattice parameters with the hyperfine parameters (spin and valence
143 states) of iron in bridgmanite and to better constrain the effect of Fe and Al on its
144 density and sound velocity in the lower mantle, direct examinations of the hyperfine,
145 lattice, and EoS parameters of high-quality Fe-bearing and (Fe,Al)-bearing single-
146 crystal bridgmanite with well characterized iron valence states, site occupancy, spin
147 states, and crystal chemistry are needed to provide new insights into these
148 aforementioned outstanding issues. In this study, we have performed high-pressure
149 synchrotron XRD and SMS measurements on two single-crystal bridgmanite samples
150 ($Mg_{0.95}Fe_{0.06}Si_{0.99}O_3$ and $Mg_{0.89}Fe_{0.12}Al_{0.11}Si_{0.89}O_3$) up to 130 GPa and 300 K. SMS is
151 used as a unique probe to determine hyperfine parameters and to infer the spin and
152 valence states of Fe in the single-crystal samples at lower-mantle pressures, while
153 analysis of high quality single-crystal XRD data reveals local lattice parameters and
154 bulk compression of bridgmanite crystals at high pressures. These results allow to

155 correlate the occurrence of the extremely high-quadrupole splitting of Fe^{2+} with the
156 A-site local lattice distortion in the high-spin state, and to model the effects of Fe and
157 Al on the density and bulk sound velocity profiles of bridgmanite at lower-mantle
158 pressures.
159

160 ## Experimental details

161 We synthesized single-crystal bridgmanite samples using the 5000-ton Kawai-type
162 multi-anvil apparatus at Okayama University at Misasa, Japan (Okuchi et al. 2015).
163 Fe-bearing bridgmanite with run number #5k2174 was synthesized using a mixture of
164 ground $MgSiO_3$, $Mg(OH)_2$, and ^{57}FeO in an appropriate ratio as the starting sample,
165 while the (Fe,Al)-bridgmanite with run number #5k2179 was synthesized using a
166 mixture of ground $MgSiO_3$, $Mg(OH)_2$, Al_2O_3, and ^{57}FeO (Okuchi et al. 2015). Here,
167 ^{57}Fe-enriched FeO (>95% enrichment) was used in the synthesis to enable high-
168 pressure Mössbauer spectroscopy measurements in a DAC. Each starting mixture was
169 cold-sealed into a Pt capsule, and compressed to 24 GPa. At this pressure, the material
170 was heated at 1650 ºC for 5.5 hrs for run #5k2174 and at 1750 ºC for 7 hrs for run
171 #5k2179. For each run, the synthesis temperature was determined from the power-
172 temperature relation of the cell assemblage that was calibrated using a
173 W97Re3/W97Re25 thermocouple. The obtained single crystals were examined by an
174 electron microprobe to confirm their chemical compositions and homogeneity,
175 showing a homogeneous composition of $Mg_{0.94}Fe_{0.06}Al_{0.01}Si_{0.99}O_3$ (Bm6) in run
176 #5k2174 and $Mg_{0.89}Fe_{0.12}Al_{0.11}Si_{0.89}O_3$ (Al-Bm11) in run #5k2179 (Okuchi et al.

177 2015). Considering the measurement error of the electron microprobe to be 1% and
178 the low concentration of Al_2O_3 in Bm6, the Bm6 sample can be considered as an Al-
179 free bridgmanite. Single-crystal XRD measurements performed at 1 bar and 300 K
180 proved that the synthesized single crystals in both compositions were in the silicate
181 perovskite structure (*Pbnm*). The refined cell parameters are: a = 4.7880(2) Å, b =
182 4.9339(2) Å, c = 6.8983(3) Å for Bm6 and a = 4.7867(2) Å, b = 4.9569(2) Å, c =
183 6.9141(4) Å for Al-Bm11 at ambient conditions. The full width at half maximum
184 (FWHM) for each diffraction peak of each given crystal is ~0.044º, indicating that the
185 synthesized single crystals are of a high quality.
186
187 These crystals were also analyzed using conventional Mössbauer spectroscopy at
188 ambient conditions to determine the hyperfine parameters and to refer the spin and
189 valence states of Fe in the samples. Mössbauer spectra, accumulated for 3 days for
190 each composition, were recorded at room temperature in transmission mode on a
191 constant acceleration Mössbauer spectrometer with a nominal 370 MBq ^{57}Co high
192 specific activity source in a 12 μm thick Rh matrix. The velocity scale was calibrated
193 relative to a 25 μm thick α-Fe foil using the positions certified for (former) National
194 Bureau of Standards standard reference material no. 1541. The conventional
195 Mössbauer spectra were fitted using the program MossA to Lorentzian doublets
196 according to current models in the literature, and the usual constraints were applied to
197 all doublets (equal component areas and widths) (Lin et al. 2016; Prescher et al. 2012).
198

For SMS measurements, we selected Bm6 and Al-Bm11 crystals less than 25 μm thick which were polished using a 3M diamond film and water as lubricant. The use of water during polishing was intended to prevent potential heating up and amorphisation. A sample platelet for each composition approximately 10 μm thick and 40 μm wide was loaded into a symmetric DAC equipped with a pair of beveled diamonds with 150/300 μm culet. NaCl was used as the pressure medium. The fluorescence shift of the ruby R_1 peak was used for the pressure calibration when the pressure was less than 80 GPa (Mao et al. 1986). Above 80 GPa, the ruby fluorescence peak was too broad and weak to be a reliable calibrant. We thus used the edge of the first-order Raman peak measured from one of the diamond anvils for the pressure calibration above 80 GPa (Akahama and Kawamura 2006). The SMS measurements were conducted at High Pressure Collaborative Access Team (HPCAT) of the Advanced Photon Source (APS), Argonne National Laboratory (ANL). An incident X-ray beam with an energy of 14.4125 keV and a bandwidth of 2 meV was used to excite the ^{57}Fe nuclei in the sample. An avalanche photodiode detector (APD) was used to collect the SMS signals with a typical collection time of ~4 to 6 hrs for each spectrum. Mössbauer spectra of the sample were collected with and without a stainless steel foil (~10 μm thick) with natural ^{57}Fe abundance at each given pressure in pressure steps of ~7 to 8 GPa up to 85 GPa for Bm6 and up to 130 GPa for Al-Bm11. The stainless steel foil was placed in front of the sample and used as a reference to determine the chemical shift of the Fe sites.

High-pressure XRD experiments of the single crystal samples were carried out at GeoSoilEnviroCARS (GSECARS) of the APS, ANL. We used the same batch of the single crystals of Bm6 and Al-Bm11 as in the SMS experiments. The single-crystal samples were polished down to ~5 μm in thickness and loaded into sample chambers drilled in Re gaskets in DACs equipped with a pair of beveled diamonds with 150/300 μm culet. Pt powder slightly packed to ~5 μm thick was placed next to the single-crystal bridgmanite sample to determine the pressure, while He was used as the pressure medium in the sample chamber. In total, we made two runs of XRD measurements for each composition at room temperature. Diffraction patterns of bridgmanite single crystals were collected by rotating ±15º about the vertical axis of the sample stage to allow collecting as many diffraction spots as possible. The pressure step for the measurements was ~1 to 2 GPa.

Results

The analysis of the obtained conventional Mössbauer spectra showed that 45% of the total Fe in Bm6 is Fe^{3+} with QS = 0.32 mm/s and CS = 0.24 mm/s, while the remaining 55% Fe is in Fe^{2+} with QS = 1.63 mm/s and CS = 1.16 mm/s. Fe in Al-Bm11 is dominated by 80% Fe^{3+} with QS = 0.92 mm/s and CS = 0.46 mm/s. Only 20% Fe in Al-Bm11 is Fe^{2+} with QS = 1.79 mm/s and CS = 1.20 mm/s.

The obtained SMS spectra of Bm6 between 1 and 13 GPa are characterized by two time beats (Fig. 1). It should be noted that the spectra of Bm6 start to change greatly

from 13 GPa to 32 GPa with more time beats observed. Above 32 GPa and up to 85 GPa, four time beats were observed for Bm6, indicating the presence of a high quadrupole splitting (QS) component in the sample. In contrast to Bm6, the SMS spectra of Al-Bm11 only exhibit a slight change with increasing pressure up to 130 GPa (Fig. 2). Below 29 GPa, there is only a broad time beat observed in the SMS spectra of Al-Bm11, whereas the spectra change to exhibit two broad time beats between 29 and 130 GPa.

The Mössbauer spectra of both Bm6 and Al-Bm11 were analyzed using the CONUSS program to derive the hyperfine parameters and doublet abundances at high pressures (Figs. 1 and 2) (Sturhahn 2000). The SMS spectra for Bm6 can be well represented using a three-doublets model (Fig. 3). According to our derived QS and chemical shift (CS) values at 1 bar and literature results at ambient conditions, doublet 1 with QS = 1.63 mm/s and doublet 2 with QS = 1.50 mm/s at ambient conditions were assigned to be the HS Fe^{2+} in the A-site, whereas doublet 3 with an extremely low QS value of 0.44 mm/s was assigned to be the HS Fe^{3+} in the A-site (Table S1) (Dyar et al. 2006). A-site Fe^{2+} accounts for 66% of the total Fe in Bm6, which is in general agreement with the conventional Mössbauer results at ambient conditions. Combining the Mössbauer and electron microprobe results, the chemical formula for Bm6 is $Mg_{0.94}Fe_{0.04}^{2+}Fe_{0.02}^{3+}Al_{0.01}Si_{0.99}O_3$. We have kept the abundances of Fe^{2+} and Fe^{3+} constant for high-pressure spectral modelling. With increasing pressure, QS of doublet 1 exhibits a dramatic increase to 3.6 mm/s between 13 GPa and 32 GPa and only a

slightly increase with pressure to 4 mm/s up to 85 GPa. Although QS of doublet 2 for Bm6 also exhibits an abrupt increase between 13 GPa and 32 GPa, the variation of QS for doublet 2 with increasing pressure is much less than doublet 1. The abundance of doublet 2 significantly decreases with pressure between 13 and 32 GPa and is accompanied by an increase in the abundance of doublet 1, with a higher QS component at high pressures.

A three-doublet model was also used to fit the SMS spectra of Al-Bm11 (Fig. 3). Doublet 1 with QS = 2.90 mm/s and doublet 2 with QS = 1.69 mm/s at 4 GPa were assigned to be the HS Fe^{2+} in the A-site, whereas doublet 3 with QS = 0.66 mm/s was assigned to be the HS Fe^{3+} based on literature results (Table S1) (Dyar et al. 2006). The total abundance of A-site Fe^{2+} is ~20%, which is consistent with the conventional Mössbauer results and does not change with increasing pressure. The chemical formula for Al-Bm11 can thus be written as $Mg_{0.89}Fe_{0.024}^{2+}Fe_{0.096}^{3+}Al_{0.11}Si_{0.89}O_3$ by combining the Mössbauer and electron microprobe results. For both doublet 1 and 2, their QS values show a weak increase with pressure, and the total abundance of doublet 1 and doublet 2 remains constant with increasing pressure. The conversion from the lower QS component to the higher QS component shown in Bm6 is not observed in Al-Bm11 (Fig. 3). Previous experimental studies have shown that addition of Al can cause an apparent increase in the volume of bridgmanite (Andrault et al. 2001; Boffa Ballaran et al. 2012). We speculate that the presence of Al also decreases the difference in volume between the sites hosting Fe^{2+} with high QS (doublet 1) and

287 those hosting Fe^{2+} with low QS (doublet 2). As a result, the enthalpy of doublet 2 in
288 our Al-Bm11 could be smaller than that of doublet 1 in the entire lower-mantle
289 pressure range. The conversion from the low-QS doublet 2 to the high QS doublet 1
290 thus does not occur in Al-Bm11. In addition, QS of doublet 3 only exhibits a weak
291 increase with pressure up to 130 GPa.
292
293 Single-crystal XRD patterns were collected from ambient conditions to pressures of
294 85 GPa for Bm6 and 110 GPa for Al-Bm11 at 300 K. The FWHM for each peak in
295 our collected XRD patterns slightly increases from 0.044° at ambient conditions to
296 ~0.059° at the maximum experimental pressure (Fig. S2), indicating the collected
297 single-crystal XRD patterns are of a high crystal quality in a quasi-hydrostatic helium
298 pressure medium. The obtained unit cell volumes of both Bm6 and Al-Bm11 exhibit
299 a continuous decrease with increasing pressure (Fig. 4 and Table S2). Comparison of
300 the obtained P-V relationships of Bm6 and Al-Bm11 to single-crystal Mg-Bm data
301 shows no abrupt variation in the unit cell volume as a function of pressure. The P-V
302 data for each given sample were fitted to the 3rd-order Birch-Murnaghan EoS (Fig.
303 4). For Bm6, we fixed V_0 = 162.96(±0.01) Å^3 as determined by XRD measurements
304 at ambient conditions and K_{0T}' = 4, yielding K_{0T} = 255(±2) GPa. For Al-Bm11, K_{0T}
305 was determined to be 264(±2) GPa with K_{0T}' = 4 (fixed) and V_0 = 164.05(±0.01) Å^3
306 (fixed). We also constructed the confidence ellipses to demonstrate the trade-off
307 between the derived K_{0T} and K_{0T}' for Bm6 and Al-Bm11 without fixing the K_{0T}' value
308 (Fig. 5).

309

310 # Discussion

311 ## Hyperfine parameters, spin states and lattice of bridgmanite

312 As shown in our Mössbauer results, QS and CS of both doublets 1 and 2, assigned to
313 be the A-site Fe^{2+} at ambient conditions, exhibit an abrupt increase between 13 and 32
314 GPa, and QS of doublet 1 in Bm6 has an extremely high value of 3.5-4.0 mm/s
315 between 32 and 85 GPa (Fig. 3 and Table S1). The observed dramatic increase in QS
316 and the occurrence of the extremely high-QS component in Fe-bearing bridgmanite
317 are consistent with previous experimental results using both SMS and conventional
318 Mössbauer spectroscopy (Jackson et al. 2005; Li et al. 2006; Lin et al. 2012;
319 McCammon et al. 2010; McCammon et al. 2013; McCammon et al. 2008; Narygina
320 et al. 2010; Potapkin et al. 2013). Some previous studies interpreted the appearance
321 of the new extremely high-QS component as the HS to IS spin transition of Fe^{2+} in the
322 A-site (Table 1) (McCammon et al. 2010; McCammon et al. 2013; McCammon et al.
323 2008; Narygina et al. 2010; Potapkin et al. 2013). One of the main experimental
324 supports for the presence of the IS state in the A-site Fe^{2+} is based on the observation
325 of a partial collapse of the Kβ satellite peak and a decrease in the derived spin moment
326 in high-pressure X-ray emission spectroscopy (XES) measurements (Badro et al. 2004;
327 Kupenko et al. 2014; Li et al. 2004; Mao et al. 2011; McCammon et al. 2010;
328 McCammon et al. 2013; McCammon et al. 2008; Narygina et al. 2010; Potapkin et al.
329 2013). However, the partial collapse of the Kβ satellite peak at high pressures could
330 be interpreted as an artifact of the pressure-induced broadening of the XES spectra

under non-hydrostatic conditions in the cold-compressed samples (Lin et al. 2016; Mao et al. 2014). Recent high-pressure synchrotron XES and SMS measurements on Fe-bearing bridgmanite with 38% Fe, showed the presence of an extremely high QS Fe^{2+} component (4.15 mm/s) at 126 GPa together with a partial collapse in the Kβ satellite peak (Dorfman et al. 2015). However, the spin moment for Fe-bearing bridgmanite with 38% Fe is approximately constant with increasing pressure once the pressure-induced broadening effect is corrected using the integrated relative difference method (Dorfman et al. 2015). These indicate that the occurrence of the extremely high QS Fe^{2+} component is not a result of HS to IS spin transition in bridgmanite at lower-mantle pressures (Dorfman et al. 2015; Mao et al. 2014). Importantly, a combined XES and SMS study on (Fe,Al)-bearing bridgmanite with a composition of relevance to the lower mantle showed that both Fe^{2+} and Fe^{3+} predominantly occupy the A site of the crystal lattice and remain in the high-spin state at lower mantle conditions (Lin et al., 2016).

Furthermore, theoretical studies suggest that the QS value of IS Fe^{2+} should be between 0.8 and 1.6 mm/s at lower-mantle pressures (Bengtson et al. 2009; Hsu et al. 2010), which is much lower than the QS values observed for both doublets 1 and 2 in Bm6 and results in previous Mössbauer studies (Lin et al. 2012; McCammon et al. 2010; McCammon et al. 2013; McCammon et al. 2008; Narygina et al. 2010; Potapkin et al. 2013). Furthermore, the IS Fe^{2+} in the A-site is theoretically predicted to be not energetically favorable (Bengtson et al., 2009; Hsu et al., 2010; Hsu and Wentzcovitch,

353 2014). A dramatic increase in the QS value of the A-site Fe^{2+} in bridgmanite should
354 be associated with the enhanced lattice distortion but not a change in the spin state
355 (Bengtson et al. 2009a; Hsu et al. 2010; Hsu and Wentzcovitch 2014). In addition, QS
356 of both doublets 1 and 2 in Al-Bm11 which were assigned to be the HS Fe^{2+} at ambient
357 conditions only shows a weak increase with pressure (Fig. 3). In particular, QS of
358 doublet 1 in Al-Bm11 is as high as 3-3.3 mm/s at lower mantle pressures. A recent
359 high pressure-temperature XES study using the same Al-Bm11 sample has shown that
360 the spin moment of Al-Bm11 is approximately constant with increasing pressure,
361 indicating no change in the spin state of Fe^{2+} in Al-Bm11 at lower-mantle pressures
362 (Lin et al. 2016). Together with recent theoretical results, we thus conclude that the
363 A-site Fe^{2+} in both Fe-bearing and (Fe,Al)-bearing bridgmanite should remain in the
364 HS state at lower-mantle pressures, and the HS to IS crossover of the A-site Fe^{2+} will
365 not occur in bridgmanite (Bengtson et al. 2009; Hsu et al. 2010; Hsu and Wentzcovitch
366 2014; Lin et al. 2016).
367
368 As shown in the Mössbauer analysis, both of our Bm6 and Al-Bm11 contain a certain
369 amount of Fe^{3+} (Fig. 3). The QS value of Fe^{3+} in Bm6 and Al-Bm11 weakly increases
370 with pressure and is less than 1 mm/s up to 130 GPa, which is significantly lower than
371 that of the LS Fe^{3+} in bridgmanite (Fig. 3 and Table S1) (Catalli et al. 2010; Catalli et
372 al., 2011; Hsu et al. 2011; Lin et al. 2012; Lin et al. 2013; Lin et al. 2016; Mao et al.
373 2011). This indicates that Fe^{3+} should reside in the A-site in both Bm6 and Al-Bm11
374 crystals and stay in the HS state at lower-mantle pressures. Since our Bm6 contains

375 minor amount of Al, the A-site Fe^{3+} should be incorporated by the coupled substitution
376 of Al^{3+} with Mg^{2+} and Si^{4+} as well as the Mg vacancies, yielding a charge balance
377 considering the uncertainties of the measurements (Boffa Ballaran et al. 2012; Frost
378 and Langenhorst 2002; Hummer and Fei 2012; Lauterbach et al. 2000; McCammon
379 1997; Potapkin et al. 2013). In Al-Bm11, Fe^{3+} is incorporated by the coupled
380 substitution of Al^{3+} to replace Mg^{2+} and Si^{4+} (Boffa Ballaran et al. 2012; Frost and
381 Langenhorst 2002; Irifune et al. 1996; Lauterbach et al. 2000; McCammon 1997;
382 Potapkin et al. 2013).
383
384 Combining the SMS with XRD results, we then investigated how the dramatic
385 increase in the QS value and the presence of the extremely high QS component of
386 the A-site Fe^{2+} would be associated with the EoS and lattice parameters of lower-
387 mantle bridgmanite. Comparison of the obtained P-V relations of our single-crystal
388 Bm6 to Mg-Bm shows that the unit cell volume of Bm6 decreases continuously with
389 pressure and does not exhibit any anomalous change (Fig. 4), indicating that the
390 dramatic increase in the QS value of Fe^{2+} between 13 and 32 GPa does not affect the
391 bulk unit cell volume of bridgmanite at lower-mantle pressures. This is also
392 consistent with recent theoretical predictions (Shukla et al. 2015). Recent studies
393 have reported a decrease in the unit cell volume of bridgmanite and an increase in
394 the bulk modulus after a volume collapse that was proposed to be associated with
395 the spin transition of B-site Fe^{3+} and/or the enhanced lattice distortion of A-site Fe^{2+}
396 at high pressures (Hsu et al. 2011; Mao et al. 2011; Mao et al. 2015). The observed

abnormal changes in the P-V data and the bulk modulus in previous studies should only be caused by the spin transition of the B-site Fe^{3+} (Hsu et al. 2011; Mao et al. 2011; Mao et al. 2015; Tsuchiya and Wang 2013).

We have further evaluated the diffraction results using previously reported models (Fig. 6) (O'keeffe and Hyde 1977). Here, the unit cell volume of a centro-symmetrically distorted ABX_3 in perovskite structure (space group *Pbnm*, Z = 4), such as bridgmanite, can be described as follows (O'keeffe and Hyde 1977; Zhao et al. 1993):

$$V = a \cdot b \cdot c = 32\left[B - X\right]^3 \cos^2 \Phi \quad (1)$$

where [*B*-*X*] is the bond length of the octahedra, and ϕ is the titling angle of the pseudo-three-fold axis of the octahedra. Although [*B*-*X*] and ϕ were calculated for the octahedra in bridgmanite, the variation in the bond length and titling angle of the octahedra is expected to affect the related properties of the large dodecahedra. [*B*-*X*] and ϕ of perovskite in orthorhombic structures can be approximated from the lattice parameters (O'keeffe and Hyde 1977; Zhao et al. 1993):

$$\left[B - X\right] = b \cdot c / (4a)$$

$$\phi = cos^{-1}(\sqrt{2}a^2/bc) \quad (2)$$

For Bm6, [*B*-*X*] decreases linearly with increasing pressure, but the slope of [*B*-*X*] changes around 40 GPa (Fig. 6). ϕ of Bm6 exhibits an anomalous softening around 40 GPa. In contrast to Bm6, [*B*-*X*] and ϕ of Al-Bm11 vary continuously with

pressure. Comparison of the calculated [*B*-*X*] and ϕ of Bm6 to those of Al-Bm11 shows that the anomalous change in [*B*-*X*] and ϕ with pressure should be associated with the dramatic increase in the QS value of Fe^{2+} in the A-site with the enhanced Jahn-Teller effect, which has been observed in Bm6 but is absent in Al-Bm11 based on the SMS results (Fig. 6). It is also interesting to note that the observed anomalous change in [*B*-*X*] and ϕ of Bm6 with pressure shown in the XRD data occurs at a higher pressure than that from the SMS results (Fig. 6).

We have also calculated [*B*-*X*] and ϕ of the single-crystal P-V data reported by Boffa Ballaran et al. (2012) to compare with our results (Fig. 6). Both [*B*-*X*] and ϕ of Fe-bearing bridgmanite (Bm4) in Boffa Ballaran et al. (2012) show a similar abnormal change with pressure as our Bm6, whereas [*B*-*X*] and ϕ of (Fe,Al)-bridgmanite ($Mg_{0.60}Fe_{0.41}Al_{0.36}Si_{0.62}O_3$, Al-Bm41) in Boffa Ballaran et al. (2012) follow a similar trend with pressure as those of our Al-Bm11. Although the spin and valence states of Fe in bridgmanite were not determined in Boffa Ballaran et al. (2012), the enhanced lattice distortion of Fe^{2+} should also occur in Bm4 of Boffa Ballaran et al. (2012) but is absent in their Al-Bm41. The difference in the calculated [*B*-*X*] and ϕ between Bm4 in Boffa Ballaran et al. (2012) and Bm6 in this study could be caused by the difference in the Fe^{2+} and Fe^{3+} as well as Al contents of the synthesized crystals, leading to their different axial compression behaviors (Fig. S3).

The spontaneous shear strain, e_4, of bridgmanite at lower-mantle pressures has also

441 been evaluated from our high-pressure XRD data (Fig. 6). e_4 has been used to
442 describe the structural change of minerals in the perovskite structure that relates the
443 M_3^+ and R_4^+ tilting with the Jahn-Teller distortions using the complete Landau
444 expansion (e.g. Carpenter et al. 2001; Fujishita et al. 2010; Ozaki et al. 2011; Tange
445 et al. 2012; Wang et al. 2015). The M_3^+ and R_4^+ distortion are associated with the tilt
446 of octahedra around the *b* and *a* axis of the orthorhombic unit cell, respectively.
447 Analysis of the derived e_4 of Al-Bm11 shows a continuous increase with pressure,
448 consistent with previous results for single-crystal Mg-Bm and Al-Bm41 in Boffa
449 Ballaran et al. (2012). A softening in e_4 of our Bm6 occurs between 30 and 50 GPa,
450 which should be related to the enhanced lattice distortion of Fe^{2+} in the A-site.
451 Similar softening in e_4 has also been identified in Bm4 in Boffa Ballaran et al.
452 (2012), although the reduction in e_4 of Bm4 between 40 and 50 GPa is much less
453 than that observed in our Bm6. The sudden change in the QS of Bm6 from the SMS
454 measurements occurs at a lower pressure than the structural change shown in XRD
455 results, which could be a result of using different pressure media and calibrants. In
456 addition, we have also calculated [*B*-*X*], ϕ, and e_4 of bridgmanite at high pressures
457 using literature data from polycrystalline samples (Figs. S4 and S5) (Andrault et al.
458 2001; Catalli et al. 2010; Catalli et al. 2011; Dorfman et al. 2013; Lundin et al. 2008;
459 Mao et al. 1991; Nishio-Hamane et al. 2008). These parameters are much more
460 scattered than those from single-crystal measurements, likely due to low-resolution
461 XRD data. Any potential anomalous change in [*B*-*X*], ϕ, and e_4 thus cannot be
462 identified from the polycrystalline data.

463

464 Combining our high-pressure SMS and XRD results and recent XES analysis
465 (Dorfman et al. 2015; Lin et al. 2016), we conclude that both A-site Fe^{2+} and Fe^{3+}
466 remain in the HS state at lower-mantle pressures. The presence of the extremely high
467 QS component of the A-site Fe^{2+} in Fe-bearing bridgmanite can be explained as a
468 result of the enhanced lattice distortion (Figs. 3 and 6) (Bengtson et al. 2009; Hsu et
469 al. 2010; Hsu and Wentzcovitch 2014). The presence of the extremely high QS
470 component of Fe^{2+} in Fe-bearing bridgmanite is associated with the conversion
471 between the low QS component to the high QS component because of the crossover
472 of the enthalpy between these two components. Theoretical calculations showed that
473 these components of the HS Fe^{2+} have different energies, bond lengths, lattice
474 parameters, *d*-orbital occupancies, and QS values (Bengtson et al. 2009; Hsu et al.
475 2014). The conversion between doublet 2 to doublet 1 in our study can be correlated
476 with changes in the bond length and tilting angle of the octahedra and the
477 spontaneous shear strain. In contrast, the conversion from the lower QS component
478 to the higher QS component is not shown in Al-Bm11 (Fig. 3). Previous
479 experimental studies have shown that addition of Al in bridgmanite can cause an
480 apparent increase in its volume (Andrault et al. 2001; Ballaran et al. 2012). The
481 presence of Al may decrease the difference in volume between the iron site with a
482 high QS and the doublet 2 site with a low QS. As a result, the enthalpy of the high
483 QS component in our Al-Bm11 could be smaller than that of the low QS component
484 throughout the whole lower-mantle pressure range. This helps explain why the

485 conversion from the low-QS doublet 2 to the high QS doublet 1 does not occur in
486 Al-Bm11.
487
488 **Effect of Fe and Al on the EoS parameters of bridgmanite**
489 Using our XRD results together with literature data, we have further investigated the
490 effect of Fe and Al on the density, bulk modulus, and bulk sound velocity of
491 bridgmanite (Figs. 7 and 8) (Andrault et al. 2001; Boffa Ballaran et al. 2012; Catalli
492 et al. 2011; Lundin et al. 2008; Mao et al. 1991; Nishio-Hamane et al. 2008). We focus
493 our discussion on the Fe-diluted bridgmanite with up to 15% Al because the Fe and
494 Al content in the crystal is believed to be ~10% in the lower mantle (Irifune et al.
495 2010). The obtained ρ_0 and K_{0T} of our Bm6 and Al-Bm11 were firstly compared to the
496 literature values of bridgmanite that did not display apparent abnormal changes in the
497 P-V relationships (Andrault et al. 2001; Boffa Ballaran et al. 2012; Catalli et al. 2011;
498 Catalli et al. 2010; Lundin et al. 2008; Mao et al. 1991).
499
500 ρ_0 of Fe-bearing bridgmanite, which is calculated from XRD measurements and
501 electron microprobe analysis, exhibits a linear increase with its Fe content (Fig. 7)
502 (Andrault et al. 2001; Boffa Ballaran et al. 2012; Catalli et al. 2010; Dorfman et al.
503 2013; Lundin et al. 2008; Mao et al. 1991; Mao et al. 2015). Comparing ρ_0 of our
504 single-crystal Al-Bm11 to that of the corresponding Fe-bearing bridgmanite with the
505 same amount of Fe shows that the presence of Al produces a decrease in the density
506 of bridgmanite (Fig. 7). However, previous studies have shown a greater reduction in

507 ρ_0 by the presence of Al in bridgmanite using Fe-bearing bridgmanite with the same
508 amount of Fe as the reference (Andrault et al. 2001; Catalli et al. 2011; Nishio-Hamane
509 and Yagi 2009; Saikia et al. 2009). It is worth noting that ρ_0 of bridgmanite in previous
510 studies was determined from decompressed polycrystalline samples at ambient
511 conditions (Andrault et al. 2001; Catalli et al. 2011; Nishio-Hamane and Yagi 2009).
512 During the decompression, the powder bridgmanite sample was normally not laser-
513 annealed to avoid the potential transformation to low-pressure phases or amorphous
514 state. XRD peaks collected during the decompression are normally quite broad, which
515 could result in much larger uncertainties on the derived volume and density of
516 bridgmanite at ambient conditions. Using well-characterized and chemically
517 homogeneous single-crystal bridgmanite samples thus allows us to provide more
518 reliable constraints on the ρ_0. ρ_0 in Saikia et al. (2009) was also determined from XRD
519 measurements and electron microprobe analysis of a single-crystal bridgmanite. The
520 different trend in ρ_0 with increasing Fe content between Saikia et al. 2009 and this
521 study could be caused by the presence of water. (Fe,Al)-bearing bridgmanite has been
522 reported to accommodate up to 1 wt.% water as structurally-bond hydroxyl (Inoue et
523 al. 2012). Synthesis of bridgmanite crystals in hydrous conditions using melt as a flux
524 can help to grow larger crystals (Boffa Ballaran et al. 2012; Saikia et al. 2009; Okuchi
525 et al. 2015). We note that the water content was not examined for the synthesized
526 single crystals in Saikia et al. (2009). The presence of water can also lower the density
527 of bridgmanite which may help reconcile the conflicting results between our and
528 literature results (Saikia et al. 2009).

529

530 Comparing K_{0T} of bridgmanite between different studies using literature values can
531 be problematic due to the use of different pressure calibrants in these studies (Andrault
532 et al. 2001; Boffa Ballaran et al. 2012; Catalli et al. 2011; Catalli et al. 2010; Lundin
533 et al. 2008; Mao et al. 1991). To be able to directly compare K_{0T} between different
534 studies, we have re-calculated the experimental pressures in all previous studies
535 without an apparent abnormal change in the P-V data using the internally consistent
536 pressure scale in Fei et al. (2007) to determine the EoS parameters of bridgmanite. For
537 studies that used Au as the pressure calibrant, pressures were re-calculated using the
538 Au pressure scale in Fei et al. (2007), which has provided an internally consistent Pt
539 scale used in this study (Catalli et al. 2011; Catalli et al. 2010; Lundin et al. 2008; Mao
540 et al. 1991). Although Andrault et al. (2001) and Boffa Ballaran et al. (2012) used
541 ruby as the pressure calibrant, we have re-calibrated the pressures in those two studies
542 using the Ruby pressure scale in Dewaele et al. (2004), which is most consistent with
543 the metal pressure scales in Fei et al. (2007) and with the use of He medium in our
544 study. We then fitted the literature P-V data using the 3rd order Birch-Murnaghan EoS
545 with fixed $K_{0T}' = 4$ and fixed V_0 from XRD measurements at ambient conditions. The
546 purpose of fixing the value of K_{0T}' is to minimize the influence of the tradeoff between
547 K_{0T} and K_{0T}' when comparing K_0 between different studies. The error ellipses for each
548 literature P-V data have been calculated to show the trade-off between K_{0T} and K_{0T}'
549 (Fig. 8)

550

We found that K_{0T} of Fe-bearing bridgmanite, 253 (±3) GPa, is independent of the Fe content within experimental uncertainties (Andrault et al. 2001; Boffa Ballaran et al. 2012; Lundin et al. 2008; Mao et al. 1991) (Fig. 7). Here, our high-quality single-crystal XRD results show an increase in K_{0T} in the Fe-diluted system by the addition of Al using Fe-bearing bridgmanite as the reference. Andrault et al. (2001) also showed that the presence of Al increases K_{0T} of bridgmanite compared to the corresponding Fe-bearing phase. Yet other two studies that also used polycrystalline samples suggested a reduction of K_{0T} with Al substitution (Fig. 7 and Fig. S6) (Catalli et al. 2011; Nishio-Hamane et al. 2008). Single-crystal bridgmanite with higher Fe and Al contents also has a K_{0T} value much lower than its Fe-bearing counterpart (Fig. S6) (Boffa Ballaran et al. 2012). We note that K_{0T} of the lower-mantle ferropericlase exhibits a weak positive dependence on the Fe content, though it starts to decrease once the Fe content is greater than 20 mol.% (Jacobsen et al. 2002), indicating that the enrichment of Fe may lead to a reduction in K_{0T}. Whether K_{0T} of (Fe,Al)-bearing bridgmanite exhibits a similar dependence on the Fe content to ferropericlase or not needs to be investigated in future studies using high-quality single crystals. In addition, the limited pressure of the experiments by Saikia et al. (2009), which resulted in a high K_{0T}' value of 5-6.3, may reduce the reliability of their constraints on the EoS parameters.

Implications

Using the obtained EoS parameters, we modeled ρ and V_Φ of bridgmanite at lower-

573 mantle pressures. The temperature effect is not included because the experimental
574 studies on the thermal EoS parameters of bridgmanite are limited, and it is unclear
575 how the compositional variation affects the thermal EoS parameters (Fiquet et al. 2000;
576 Tange et al. 2012; Wolf et al. 2015). Bridgmanite in the lower mantle is expected to
577 have an average composition of $(Mg_{0.9}Fe_{0.1})(Al_{0.1}Si_{0.9})O_3$ (Al-Bm10), which is used
578 as the reference to understand how the enrichment of Fe and/or Al influences ρ and
579 V_Φ. We firstly modeled the ρ and V_Φ profiles of bridgmanite with a composition of
580 $(Mg_{0.8}Fe_{0.2})(Al_{0.1}Si_{0.9})O_3$ in which half of the total Fe is Fe^{2+}. Our modeling results
581 show that $(Mg_{0.8}Fe_{0.2})(Al_{0.1}Si_{0.9})O_3$-bridgmanite has a 2.5(±0.2)% greater ρ but a
582 1.3(±0.7)% lower V_Φ than Al-Bm10 (Fig. 9). In this case, the enrichment of Fe in
583 bridgmanite will exhibit a seismic signature of greater ρ but lower V_Φ. The enrichment
584 of Al should occur with the increase in the amount of A-site Fe in bridgmanite through
585 the coupled substitution of Al and Fe with Mg and Si. We have also calculated ρ and
586 V_Φ of $(Mg_{0.8}Fe_{0.2})(Al_{0.2}Si_{0.8})O_3$-bridgmanite which is enriched in both Al and Fe. We
587 simply assumed that $(Mg_{0.8}Fe_{0.2})(Al_{0.2}Si_{0.8})O_3$-bridgmanite has a similar K_{0T} to our
588 Al-Bm11 due to complex behavior of Fe on K_{0T} of (Fe,Al)-bearing bridgmanite. Our
589 modeling results show that increasing the Fe and Al content in bridgmanite up to 20%
590 $[(Mg_{0.8}Fe_{0.2})(Al_{0.1}Si_{0.9})O_3]$ will lead to a ρ ~1.5% greater than that of Al-Bm10 in the
591 lower mantle. Meanwhile, the combined effect of Al and Fe enrichment will produce
592 a 0.1-0.5(±0.7)% increase in V_Φ. V_Φ of bridgmanite, which is enriched in both Al and
593 Fe, is indistinguishable from that of Al-Bm10 considering the calculation
594 uncertainties.

595

596 Combining our synchrotron XRD and SMS measurements on single-crystal
597 bridgmanite and together with literature XES results (Dorfman et al. 2015; Lin et al.
598 2016), we conclude that A-site Fe^{2+} in Fe-bearing bridgmanite will be in the HS state
599 in the Earth's lower mantle. For Fe-bearing bridgmanite, the enhanced lattice
600 distortion of A-site Fe^{2+} will occur at the top of the lower mantle, resulting in an
601 extremely high QS value of 3.5-4 mm/s. The presence of the extremely high QS Fe^{2+}
602 component does not affect the variation of the unit cell volume with pressure but is
603 associated with changes in the bond length, titling angle of the octahedra, and the
604 spontaneous shear strain. Although previous studies attributed the presence of the
605 extremely high QS Fe^{2+} component to be a result of the HS to IS spin transition which
606 is mainly supported by the partial collapse of the Kβ satellite peak from the XES
607 measurements, recent high pressure-temperature XES studies showed that the partial
608 collapse of the Kβ satellite peak is only an artifact of the peak broadening at high
609 pressures (Dorfman et al. 2015; Lin et al. 2016; Mao et al. 2014). Our results support
610 the notion that the intermediate-spin state of the A-site Fe^{2+} will not occur in
611 bridgmanite at relevant pressure and temperature conditions of the lower mantle. In
612 (Fe,Al)-bridgmanite where Al is expected to substitute into B-site, the enhanced
613 lattice distortion of A-site Fe^{2+} is absent. Our XRD and SMS results thus provide
614 crucial constraints on the Fe spin states, lattice and the EoS parameters of bridgmanite
615 at relevant pressure conditions of the lower mantle. More importantly, we further
616 discussed the effect of compositional variation on the ρ and V_Φ profiles of the lower-

617 mantle bridgmanite using the obtained EoS parameters. Our modeling results have
618 shown that the enrichment of Fe will cause an enhanced ρ and a reduced V_Φ in
619 bridgmanite, whereas the Al and Fe enrichment in bridgmanite will exhibit a seismic
620 signature of higher ρ, but a V_Φ profile undistinguishable from bridgmanite with an
621 average mantle composition within calculation uncertainties. These modeling results
622 are crucial for understanding the potential chemical cause for the observed seismic
623 anomalies in the Earth's lower mantle.
624

625 ## Acknowledgement

626 We acknowledge J. Liu for XRD measurements, C. McCammon for conventional
627 Mössbauer measurements and data analysis, and H. Hsu for thoughtful discussion. Z.
628 Mao acknowledges financial support from the National Natural Science Foundation
629 of China (41522403), National Basic Research Program of China (2014CB845904),
630 and the Fundamental Research Funds for the Central Universities in China
631 (WK2080000052). J. F. Lin acknowledges support from the US National Science
632 Foundation (EAR-1446946). Portions of this work were performed at
633 GeoSoilEnviroCARS, Advanced Photon Source, Argonne National Laboratory.
634 GSECARS was supported by the National Science Foundation (EAR-0622171) and
635 Department of Energy (DE-FG02-94ER14466) under Contract No. DE-AC02-
636 06CH11357. Portions of this work were performed at HPCAT (Sector 16) of the
637 Advanced Photon Source (APS), Argonne National Laboratory. HPCAT is supported
638 by CIW, CDAC, UNLV, and LLNL through funding from DOE-NNSA, DOE-BES

639 and NSF. APS is supported by DOE-BES, under Contract No. DE-AC02-06CH11357.

640

641 References

642 Akahama, Y., and Kawamura, H. (2006) Pressure calibration of diamond anvil Raman
643 gauge to 310 GPa. Journal of Applied Physics, 100, doi: 10.1063/1.2335683.
644 Andrault, D., Bolfan-Casanova, N., and Guignot, N. (2001) Equation of state of lower
645 mantle (Al,Fe)-$MgSiO_3$ perovskite. Earth and Planetary Science Letters, 193, 501-508.
646 Badro, J., Rueff, J.P., Vanko, G., Monaco, G., Fiquet, G., and Guyot, F. (2004)
647 Electronic transitions in perovskite: Possible nonconvecting layers in the lower mantle.
648 Science, 305, 383-386.
649 Boffa Ballaran, T., Kurnosov, A., Glazyrin, K., Frost, D.J., Merlini, M., Hanfland, M.,
650 and Caracas, R. (2012) Effect of chemistry on the compressibility of silicate
651 perovskite in the lower mantle. Earth and Planetary Science Letters, 333, 181-190.
652 Bengtson, A., Li, J., and Morgan, D. (2009a) Mössbauer modeling to interpret the spin
653 state of iron in (Mg,Fe)SiO3 perovskite. Geophysical Research Letters, 36, doi:
654 10.1029/2009gl038340.
655 Bengtson, A., Li, J., and Morgan, D. (2009b) Mossbauer modeling to interpret the
656 spin state of iron in (Mg,Fe)SiO_3 perovskite. Geophysical Research Letters, 36, doi:
657 10.1029/2009gl038340.
658 Carpenter, M.A., Becerro, A.I., and Seifert, F. (2001) Strain analysis of phase
659 transitions in (Ca,Sr)TiO_3 perovskites. American Mineralogist, 86, 348-363.
660 Catalli, K., Shim, S.H., Dera, P., Prakapenka, V.B., Zhao, J.Y., Sturhahn, W., Chow,
661 P., Xiao, Y.M., Cynn, H., and Evans, W.J. (2011) Effects of the Fe^{3+} spin transition on
662 the properties of aluminous perovskite-New insights for lower-mantle seismic
663 heterogeneities. Earth and Planetary Science Letters, 310, 293-302.
664 Catalli, K., Shim, S.H., Prakapenka, V.B., Zhao, J.Y., Sturhahn, W., Chow, P., Xiao,
665 Y.M., Liu, H.Z., Cynn, H., and Evans, W.J. (2010) Spin state of ferric iron in $MgSiO_3$
666 perovskite and its effect on elastic properties. Earth and Planetary Science Letters,
667 289, 68-75.
668 Dewaele, A., Loubeyre, P., and Mezouar, M. (2004) Equations of state of six metals
669 above 94 GPa. Physical Review B, 70, doi: 10.1103/Physrevb.70.094112.
670 Dorfman, S.M., Shieh, S.R., Meng, Y., Prakapenka, V.B., and Duffy, T.S. (2012)
671 Synthesis and equation of state of perovskites in the $(Mg,Fe)_3Al_2Si_3O_{12}$ system to 172
672 GPa. Earth and Planetary Science Letters, 357-358, 194-202.
673 Dorfman, S.M., Meng, J., Prakapenka, V.B., and Duffy, T.S. (2013) Effects of Fe-
674 enrichment on the equation of state and stability of (Mg,Fe)SiO_3 perovskite. Earth and
675 Planetary Science Letters, 361, 249-257.
676 Dorfman, S.M., Badro, J., Rueff, J.P., Chow, P., Xiao, Y.M., and Gillet, P. (2015)
677 Composition dependence of spin transition in (Mg,Fe)SiO_3 bridgmanite. American
678 Mineralogist, 100, 2246-2253.
679 Dyar, M.D., Agresti, D.G., Schaefer, M.W., Grant, C.A., and Sklute, E.C. (2006)

Mössbauer spectroscopy of earth and planetary materials. Annual Review of Earth and Planetary Sciences, 34, 83-125.

Fei, Y., Ricolleau, A., Frank, M., Mibe, K., Shen, G., and Prakapenka, V. (2007) Toward an interally consistent pressure scale. Proceeding of the National Academy of Sciences of the UAS, 104, 9182-9186.

Fiquet, G., Dewaele, A., Andrault, D., Kunz, M., and Le Bihan, T. (2000) Thermoelastic properties and crystal structure of $MgSiO_3$ perovskite at lower mantle pressure and temperature conditions. Geophysical Research Letters, 27, 21-24.

Frost, D.J., and Langenhorst, F. (2002) The effect of Al_2O_3 on Fe-Mg partitioning between magnesiowüstite and magnesium silicate perovskite. Earth and Planetary Science Letters, 199, 227-241.

Frost, D.J., Liebske, C., Langenhorst, F., McCammon, C.A., Tronnes, R.G., and Rubie, D.C. (2004) Experimental evidence for the existence of iron-rich metal in the Earth's lower mantle. Nature, 428, 409-412.

Fujino, K., Nishio-Hamane, D., Nagai, T., Seto, Y., Kuwayama, Y., Whitaker, M., Ohfuji, H., Shinmei, T., and Irifune, T. (2014) Spin transition, substitution, and partitioning of iron in lower mantle minerals. Physics of the Earth and Planetary Interiors, 228, 186-191.

Fujino, K., Nishio-Hamane, D., Seto, Y., Sata, N., Nagai, T., Shinmei, T., Irifune, T., Ishii, H., Hiraoka, N., Cai, Y.Q., and Tsuei, K.D. (2012) Spin transition of ferric iron in Al-bearing Mg-perovskite up to 200 GPa and its implication for the lower mantle. Earth and Planetary Science Letters, 317, 407-412.

Fujishita, H., Yamada, T., Nakada, S., Okamoto, H., Shitara, S., Kato, M., and Koike, Y. (2010) Spontaneous strain in $Ba_{0.6}Ka_{0.4}BiO_3$. Physica C-Superconductivity and Its Applications, 470, S770-S771, doi: 10.1016/j.physc.2009.11.023.

Glazyrin, K., Boffa Ballaran, T.B., Frost, D.J., McCammon, C., Kantor, A., Merlini, M., Hanfland, M., and Dubrovinsky, L. (2014) Magnesium silicate perovskite and effect of iron oxidation state on its bulk sound velocity at the conditions of the lower mantle. Earth and Planetary Science Letters, 393, 182-186.

Goncharov, A.F., Struzhkin, V.V., Montoya, J.A., Kharlamova, S., Kundargi, R., Siebert, J., Badro, J., Antonangeli, D., Ryerson, F.J., and Mao, W. (2010) Effect of composition, structure, and spin state on the thermal conductivity of the Earth's lower mantle. Physics of the Earth and Planetary Interiors, 180, 148-153.

Hemley, R.J., and Cohen, R.E. (1992) Silicate perovskite. Annual Review of Earth and Planetary Sciences, 20, 553-600.

Hirose, K. (2002) Phase transitions in pyrolitic mantle around 670-km depth: Implications for upwelling of plumes from the lower mantle. Journal of Geophysical Research-Solid Earth, 107, doi: 10.1029/2001jb000597.

Hsu, H., Blaha, P., Cococcioni, M., and Wentzcovitch, R.M. (2011) Spin-state crossover and hyperfine interactions of ferric iron in $MgSiO_3$ perovskite. Physical Review Letters, 106, doi: 10.1103/Physrevlett.106.118501.

Hsu, H., Umemoto, K., Blaha, P., and Wentzcovitch, R.M. (2010) Spin states and hyperfine interactions of iron in $(Mg,Fe)SiO_3$ perovskite under pressure. Earth and Planetary Science Letters, 294, 19-26.

Hsu, H., and Wentzcovitch, R.M. (2014) First-principles study of intermediate-spin ferrous iron in the Earth's lower mantle. Physical Review B, 90, doi: 10.1103/Physrevb.90.195205.

Hsu, H., Yu, Y.G., and Wentzcovitch, R.M. (2012) Spin crossover of iron in aluminous $MgSiO_3$ perovskite and post-perovskite. Earth and Planetary Science Letters, 359-360, 34-39.

Hummer, D.R., and Fei, Y.W. (2012) Synthesis and crystal chemistry of Fe^{3+}-bearing $(Mg,Fe^{3+})(Si,Fe^{3+})O_3$ perovskite. American Mineralogist, 97, 1915-1921.

Inoue, T., Yabuki, T., and Yurimoto, H. (2012) Water contents of Al-bearing minerals in the mantle transition zone and the lower mantle. In T. Okuchi, Ed., Joint Symposium of Misasa-2012 and Geofluid-2, p. P21-02. ISEI, Misasa, Tottori, Japan.

Irifune, T., Koizumi, T., Ando, J-I. (1996) An experimental study of the garnet-perovskite transformation in the system MgSiO3-Mg3Al2Si3O12. Physics of the Earth and Planetary Interiors, 96, 147-157.

Irifune, T., Shinmei, T., McCammon, C.A., Miyajima, N., Rubie, D.C., and Frost, D.J. (2010) Iron partitioning and density changes of pyrolite in Earth's lower mantle. Science, 327, 193-195.

Jackson, J.M., Sturhahn, W., Shen, G.Y., Zhao, J.Y., Hu, M.Y., Errandonea, D., Bass, J.D., and Fei, Y.W. (2005) A synchrotron Mössbauer spectroscopy study of $(Mg,Fe)SiO_3$ perovskite up to 120 GPa. American Mineralogist, 90, 199-205.

Kupenko, I., McCammon, C., Sinmyo, R., Prescher, C., Chumakov, A.I., Kantor, A., Ruffer, R., and Dubrovinsky, L. (2014) Electronic spin state of Fe,Al-containing $MgSiO_3$ perovskite at lower mantle conditions. Lithos, 189, 167-172, doi: 10.1016/j.lithos.2013.10.022.

Lauterbach, S., McCammon, C.A., van Aken, P., Langenhorst, F., and Seifert, F. (2000) Mössbauer and ELNES spectroscopy of $(Mg,Fe)(Si,Al)O_3$ perovskite: a highly oxidised component of the lower mantle. Contributions to Mineralogy and Petrology, 138, 17-26.

Li, J., Struzhkin, V.V., Mao, H.K., Shu, J.F., Hemley, R.J., Fei, Y.W., Mysen, B., Dera, P., Prakapenka, V., and Shen, G.Y. (2004) Electronic spin state of iron in lower mantle perovskite. Proceedings of the National Academy of Sciences of the United States of America, 101, 14027-14030.

Li, J., Sturhahn, W., Jackson, J.M., Struzhkin, V.V., Lin, J.F., Zhao, J., Mao, H.K., and Shen, G. (2006) Pressure effect on the electronic structure of iron in $(Mg,Fe)(Si,Al)O_3$ perovskite: a combined synchrotron Mössbauer and X-ray emission spectroscopy study up to 100 GPa. Physics and Chemistry of Minerals, 33, 575-585.

Lin, J.F., Alp, E.E., Mao, Z., Inoue, T., McCammon, C., Xia, Y.M., Chow, P., and Zhao, J.Y. (2012) Electronic spin states of ferric and ferrous iron in the lower-mantle silicate perovskite. American Mineralogist, 97, 592-597.

Lin, J.F., Speziale, S., Mao, Z., and Marquardt, H. (2013) Effects of the electronic spin transitions of iron in lower-mantle minerals: implications to deep-mantle geophysics and geochemistry. Review in Geophysics, 51, 2012RG000414.

Lin, J.F., Watson, H., Vanko, G., Alp, E.E., Prakapenka, V.B., Dera, P., Struzhkin, V.V., Kubo, A., Zhao, J.Y., McCammon, C., and Evans, W.J. (2008) Intermediate-spin

ferrous iron in lowermost mantle post-perovskite and perovskite. Nature Geoscience, 1, 688-691.

Lin, J.F., Mao, Z., Yang, J., Liu, J., Xiao, Y., Chow, P., and Okuchi, T. (2016) High-spin Fe^{2+} and Fe^{3+} in single-crystal aluminous bridgmanite in the lower mantle. Geophysical Research letters, 43, doi:10.1002/2016GL069836.

Lundin, S., Catalli, K., Santillan, J., Shim, S.H., Prakapenka, V.B., Kunz, M., and Meng, Y. (2008) Effect of Fe on the equation of state of mantle silicate perovskite over 1 Mbar. Physics of the Earth and Planetary Interiors, 168, 97-102.

Mao, H.K., Xu, J., and Bell, P.M. (1986) Calibration of the ruby pressure gauge to 800-Kbar under quasi-hydrostatic conditions. Journal of Geophysical Research-Solid Earth and Planets, 91, 4673-4676.

Mao, Z., Lin, J.F., Scott, H.P., Watson, H.C., Prakapenka, V.B., Xiao, Y., Chow, P., and McCammon, C. (2011) Iron-rich perovskite in the Earth's lower mantle. Earth and Planetary Science Letters, 309, 179-184.

Mao, Z., Lin, J.F., Yang, J., Inoue, T., and Prakapenka, V.B. (2015) Effects of the Fe^{3+} spin transition on the equation of state of bridgmanite. Geophysical Research Letters, 42, 4335-4342, doi: 10.1002/2015GL064400.

Mao, Z., Lin, J.F., Yang, J., Wu, J., Watson, H.C., Xiao, Y., Chow, P., and Zhao, J. (2014) Spin and valence states of iron in Al-bearing silicate glass at high pressures studied by synchrotron Mössbauer and X-ray emission spectroscopy. American Mineralogist, 99, 415-423.

McCammon, C. (1997) Perovskite as a possible sink for ferric iron in the lower mantle. Nature, 387, 694-696.

McCammon, C., Dubrovinsky, L., Narygina, O., Kantor, I., Wu, X., Glazyrin, K., Sergueev, I., and Chumakov, A.I. (2010) Low-spin Fe^{2+} in silicate perovskite and a possible layer at the base of the lower mantle. Physics of the Earth and Planetary Interiors, 180, 215-221.

McCammon, C., Glazyrin, K., Kantor, A., Kantor, I., Kupenko, I., Narygina, O., Potapkin, V., Prescher, C., Sinmyo, R., Chumakov, A., Ruffer, R., Sergueev, I., Smirnov, G., and Dubrovinsky, L. (2013) Iron spin state in silicate perovskite at conditions of the Earth's deep interior. High Pressure Research, 33, 663-672, doi: 10.1080/08957959.2013.805217.

McCammon, C., Kantor, I., Narygina, O., Rouquette, J., Ponkratz, U., Sergueev, I., Mezouar, M., Prakapenka, V., and Dubrovinsky, L. (2008) Stable intermediate-spin ferrous iron in lower-mantle perovskite. Nature Geoscience, 1, 684-687.

Murakami, M., Ohishi, Y., Hirao, N., and Hirose, K. (2012) A perovskitic lower mantle inferred from high-pressure, high-temperature sound velocity data. Nature, 485, 90-U118, doi: 10.1038/Nature11004.

Narygina, O.V., Kantor, I.Y., McCammon, C.A., and Dubrovinsky, L.S. (2010) Electronic state of Fe^{2+} in $(Mg,Fe)(Si,Al)O_3$ perovskite and $(Mg,Fe)SiO_3$ majorite at pressures up to 81 GPa and temperatures up to 800 K. Physics and Chemistry of Minerals, 37, 407-415.

Nishio-Hamane, D., Seto, Y., Fujino, K., and Nagai, T. (2008) Effect of $FeAlO_3$ incorporation into $MgSiO_3$ on the bulk modulus of perovskite. Physics of the Earth

812 and Planetary Interiors, 166, 219-225.
813 Nishio-Hamane, D., and Yagi, T. (2009) Equations of state for postperovskite phases
814 in the $MgSiO_3$-$FeSiO_3$-$FeAlO_3$ system. Physics of the Earth and Planetary Interiors,
815 175, 145-150.
816 O'keeffe, M., and Hyde, B.G. (1977) Some structures topologically related to cubic
817 perovskite (E21), ReO_3 ($D0_9$) and Cu3Au($L1_2$). Acta Crystallographica Section B-
818 Structural Science, 33, 3802-3813.
819 Okuchi, T., Purevjav, N., Tomioka, N., Lin, J.F., Kuribayashi, T., Schoneveld, L.,
820 Hwang, H., Sakamoto, N., Kawasaki, N., and Yurimoto, H. (2015) Synthesis of large
821 and homogeneous single crystals of water-bearing minerals by slow cooling at deep-
822 mantle pressures. American Mineralogist, 100, 1483-1492.
823 Ozaki, T., Kusunose, K., Yamaguchi, H., Kajiwara, K., and Chikaura, Y. (2011)
824 Spontaneous strain of conductive strontium titanate $Sr_{1-x}LaxTiO_3$ measured by using
825 X-ray topographic domain contrast. Phase Transitions, 84, 837-842.
826 Potapkin, V., McCammon, C., Glazyrin, K., Kantor, A., Kupenko, I., Prescher, C.,
827 Sinmyo, R., Smirnov, G.V., Chumakov, A.I., Ruffer, R., and Dubrovinsky, L. (2013)
828 Effect of iron oxidation state on the electrical conductivity of the Earth's lower mantle.
829 Nature Communications, 4, doi: 10.1038/Ncomms2436.
830 Prescher, C., McCammon, C., and Dubrovinsky, L. (2012) MossA: a program for
831 analyzing energy-domain Mossbauer spectra from conventional and synchrotron
832 sources. Journal of Applied Crystallography, 45, 329-331.
833 Ringwood, A.E. (1975) Composition and petrology of the Earth's mantle. 618 p.
834 McGraw-Hill, New York.
835 Saikia, A., Boffa Ballaran, T.B., and Frost, D.J. (2009) The effect of Fe and Al
836 substitution on the compressibility of $MgSiO_3$-perovskite determined through single-
837 crystal X-ray diffraction. Physics of the Earth and Planetary Interiors, 173, 153-161.
838 Shukla, G., Wu, Z.Q., Hsu, H., Floris, A., Cococcioni, M., and Wentzcovitch, R.M.
839 (2015) Thermoelasticity of Fe^{2+}-bearing bridgmanite. Geophysical Research Letters,
840 42, 1741-1749.
841 Stixrude, L., and Cohen, R.E. (1993) Stability of orthorhombic $MgSiO_3$ perovskite in
842 the Earth's lower mantle. Nature, 364, 613-616.
843 Sturhahn, W. (2000) CONUSS and PHOENIX: Evaluation of nuclear resonant
844 scattering data. Hyperfine Interactions, 125, 149-172.
845 Tange, Y., Kuwayama, Y., Irifune, T., Funakoshi, K., and Ohishi, Y. (2012) P-V-T
846 equation of state of $MgSiO_3$ perovskite based on the MgO pressure scale: A
847 comprehensive reference for mineralogy of the lower mantle. Journal of Geophysical
848 Research, 117, doi: 10.1029/2011jb008988.
849 Tsuchiya, T., Tsuchiya, J., Umemoto, K., and Wentzcovitch, R.A. (2004) Phase
850 transition in $MgSiO_3$ perovskite in the earth's lower mantle. Earth and Planetary
851 Science Letters, 224, 241-248.
852 Tsuchiya, T., and Wang, X. (2013) Ab initio investigation on the high-temperature
853 thermodynamic properties of Fe^{3+}-bearing $MgSiO_3$ perovskite. Journal of
854 Geophysical Research, 118, 83-91.
855 Vanpeteghem, C.B., Angle, R.J., Ross, N.L., Jacobsen, S.D., Dobson, D.P., Litasov,

K.D., and Ohtani, E. (2006) Al, Fe substitution in the MgSiO3 perovskite structure: A single-crystal X-ray diffraction study. Physics of the Earth and Planetary Interiors, 155, 96-103.

Wang, X.L., Tsuchiya, T., and Hase, A. (2015) Computational support for a pyrolitic lower mantle containing ferric iron. Nature Geoscience, 8, 556-559.

Wolf, A.S., Jackson, J.M., Dera, P., and Prakapenka, V.B. (2015) The thermal equation of state of (Mg, Fe)SiO_3 bridgmanite (perovskite) and implications for lower mantle structures. Journal of Geophysical Research-Solid Earth, 120, 7460-7489, doi: 10.1002/2015JB012108.

Zhao, Y.S., Weidner, D.J., Parise, J.B., and Cox, D.E. (1993) Critical phenomena and phase transition of perovskite data for $NaMgF_3$ Perovskite. Part II. Physics of the Earth and Planetary Interiors, 76, 17-34.

This is a preprint, the final version is subject to change, of the American Mineralogist (MSA)
Cite as Authors (Year) Title. American Mineralogist, in press.
(DOI will not work until issue is live.) DOI: http://dx.doi.org/10.2138/am-2017-5770

900 Table 1. Mössbauer spectroscopy results of bridgmanite at high pressures

Composition		Sample	P (GPa)	Valence state	Spin State	QS (mm/s)	Reference
Fe-bearing	$(Mg_{0.94}Fe_{0.06})SiO_3$	Single crystal	0-85	Fe^{2+}	HS	1.6-4.0	This study
				Fe^{2+}	HS	1.5-2.4	
				Fe^{3+}	HS	0.4-0.5	
	$(Mg_{0.9}Fe_{0.1})SiO_3$	Powder	42-75	Fe^{2+}	HS	3.37-3.39	Jackson et al. (2005)
				Fe^{2+}	HS	2.74-2.79	
				Fe^{3+}		1.15-1.47	
	$(Mg_{0.95}Fe_{0.05})SiO_3$	Powder	0-120	Fe^{2+}	HS	1.89-3.51	Jackson et al. (2005)
				Fe^{2+}	HS	1.59-2.75	
				Fe^{3+}		0.57-1.63	
	$(Mg_{0.88}Fe_{0.12})SiO_3$	Powder	0-120	Fe^{2+}	HS	1.8-3.5	McCammon et al. (2008)
				Fe^{2+}	IS	3.2-4.1	
				Fe^{3+}	HS	0.6-1.5	
	$(Mg_{0.6}Fe_{0.4})SiO_3$	Powder	110	Fe^{2+}	IS	4.18	Lin et al. (2008)
				Fe^{2+}	IS	3.98	
	$(Mg_{0.82}Fe_{0.18})SiO_3$	Powder	120-130	Fe^{2+}	IS	4.4	McCammon et al. (2010)
				Fe^{2+}	LS	0-0.7	
	$MgSiO_3$+10 mol.% Fe_2O_3	Powder	40-136	Fe^{3+}	HS	0.5-1	Catalli et al. (2010)
				Fe^{3+}	LS	2.8-3.6	
	$(Mg_{0.88}Fe_{0.12})SiO_3$	Powder	30-80	Fe^{2+}	IS	3.9-4.2	Narygina et al. (2010)
				Fe^{2+}	HS	2-2.7	
				Fe^{3+}	HS	0.5-1.5	
	$(Mg_{0.75}Fe_{0.25})SiO_3$	Powder	135	Fe^{2+}	IS	4.1	Mao et al. (2011)
				Fe^{3+}	LS	2.99	
				Fe^{3+}	LS	1.84	
	$(Mg_{0.9}Fe_{0.1})SiO_3$	Powder	0-120	Fe^{2+}	HS	1.82-4.1	Lin et al. (2012)
				Fe^{2+}	HS	1.54-3.1	
				Fe^{3+}	HS	0.65-2	
	$(Mg_{0.61}Fe_{0.38}Ca_{0.01})SiO_3$	Powder	126	Fe^{2+}	HS	4.18	Dorfman et al. (2015)
				Fe^{2+}	HS	3.15	
(Fe,Al)-bearing	$Mg_{0.90}Fe_{0.12}Al_{0.11}Si_{0.90}O_3$	Single crystal	4-130	Fe^{2+}	HS	2.9-3.4	This study
				Fe^{2+}	HS	1.7-1.9	
				Fe^{3+}	HS	0.7-0.9	
	$(Mg_{0.88}Fe_{0.09})(Si_{0.94}Al_{0.10})O_3$	Powder	12-100	Fe^{2+}		2.4-3.45	Li et al. (2006)
				Fe^{2+}		2.11-2.75	
				Fe^{3+}		0.54-0.74	
	$Mg_{0.88}Fe_{0.13}Al_{0.11}Si_{0.88}O_3$	Powder	25-95	Fe^{3+}	LS	3-3.8	Catalli et al. (2011)
				Fe^{3+}	LS	2.1-2.3	
				Fe^{3+}	HS	0.6-1.3	

901

Figure caption

Figure 1. Representative synchrotron Mössbauer spectra and modeled energy spectra of Bm6 at high pressures and 300 K. Red circles: experimental spectra; black lines: modeled spectra using CONUSS program (Sturhahn 2000). Left panel: sample spectra; middle panel: spectra of sample plus stainless steel; right panel: energy spectra calculated from the fits in the left panel; blue line: doublet 1; red line: doublet 2; green line: doublet 3.

Figure 2. Representative synchrotron Mössbauer spectra and modeled energy spectra of Al-Bm11 at high pressures and 300 K. Red circles: experimental spectra; black lines: modeled spectra using CONUSS program (Sturhahn 2000). Left panel: sample spectra; middle panel: spectra of sample plus stainless steel; right panel: modeled energy spectra with assigned doublets calculated from the fits in the left panel. Blue: doublet 1; red: doublet 2; green: doublet 3.

Figure 3. Derived quadrupole splitting (QS), chemical shift (CS), and relative doublet abundance of Fe in Bm6 and Al-Bm11 at high pressures, respectively. (a) Bm6; (b) Al-Bm11. Doublets 1 and 2 are assigned to be Fe^{2+}, while doublet 3 is assigned to be Fe^{3+}. Solid lines are shown for readers to follow the trend with increasing pressure.

Figure 4. Pressure-volume relationships of bridgmanite at 300 K. Red: Bm6; green circles: Al-Bm11; blue line: $MgSiO_3$ (Boffa Ballaran et al. 2012); circles: data from

924 the first run; diamonds: data from the second run. Corresponding lines represent the
925 fits using the 3rd order Birch-Murnaghan equation to the experimental results. Inserted
926 figure shows the variation of the unit-cell volume of Bm6 and Al-Bm11, respectively,
927 using Mg-Bm as the reference. Uncertainties are smaller than symbols when not
928 shown.

929

930 Figure 5. Error ellipses of K_{0T}-K_{0T}' for Bm6 and Al-Bm11 at the 1-σ level. Red: Bm6;
931 green: Al-Bm11; blue: Mg-Bm (Boffa Ballaran et al. 2012).

932

933 Figure 6. Octahedral bond length ([*B*-*X*]), octahedral tilting angles (ϕ), and Shear
934 strain component (e_4) of bridgmanite at high pressures and 300 K. (a). octahedral bond
935 length, [*B*-*X*]; (b). octahedral tilting angles, ϕ; (c). shear strain component, e_4. Red
936 solid circles and line: Bm6; green solid circles and line: Al-Bm11; blue open circles
937 and line: Bm4 (Boffa Ballaran et al. 2012); orange open circles and line: Al-Bm41
938 (Boffa Ballaran et al. 2012). Solid lines are shown for readers to follow the trend with
939 increasing pressure.

940

941 Figure 7. Density (ρ_0) and bulk modulus (K_{0T}) of bridgmanite at ambient conditions.
942 (a). ρ_0; (b). K_{0T}. Red: Fe-bearing bridgmanite; blue: (Fe,Al)-bridgmanite; open
943 symbols: results from polycrystalline bridgmanite samples (Andrault et al. 2001;
944 Catalli et al. 2010; Catalli et al. 2011; Dorfman et al. 2013; Lundin et al. 2008; Mao
945 et al. 1991); solid symbols: results from single-crystal bridgmanite samples (This

946 study; Boffa Ballaran et al. 2012; Saikia et al. 2009); stars: our Bm6 and Al-Bm11.
947 Errors are smaller than symbols when not shown.

948

949 Figure 8. Confidence ellipses of the bulk modulus (K_{0T}) and its pressure derivative
950 (K_{0T}') of bridgmanite at ambient conditions at the 1-σ level using literature data. Solid
951 lines: Fe-bearing bridgmanite; dashed lines: (Fe,Al)-bridgmanite; Blue: Bm4 (Boffa
952 Ballaran et al. 2012); green: Bm5 (Andrault et al. 2001); orange: Bm9 (Lundin et al.
953 2008); light blue: Bm9 (Dorfman et al. 2013); yellow: Bm10 (Mao et al. 1991);
954 magenta: Bm15 (Lundin et al. 2008); red: Al- Bm5 (Andrault et al. 2001); black: Al-
955 Bm13 (Catalli et al. 2011); olive: Al- Bm15 (Nishio-Hamane et al. 2009).

956

957 Figure 9. Variation of density ($\Delta\rho/\rho$) and bulk sound velocity ($\Delta V_\Phi/V_\Phi$) of bridgmanite
958 at lower-mantle pressures and 300 K using Al-Bm10 as the reference. (a). $\Delta\rho/\rho$; (b).
959 $\Delta V_\Phi/V_\Phi$. Red: $(Mg_{0.8}Fe_{0.2})(Al_{0.2}Si_{0.8})O_3$-bridgmanite; blue: $(Mg_{0.8}Fe_{0.2})(Al_{0.1}Si_{0.9})O_3$-
960 bridgmanite; grey: $(Mg_{0.9}Fe_{0.1})(Al_{0.1}Si_{0.9})O_3$-bridgmanite.

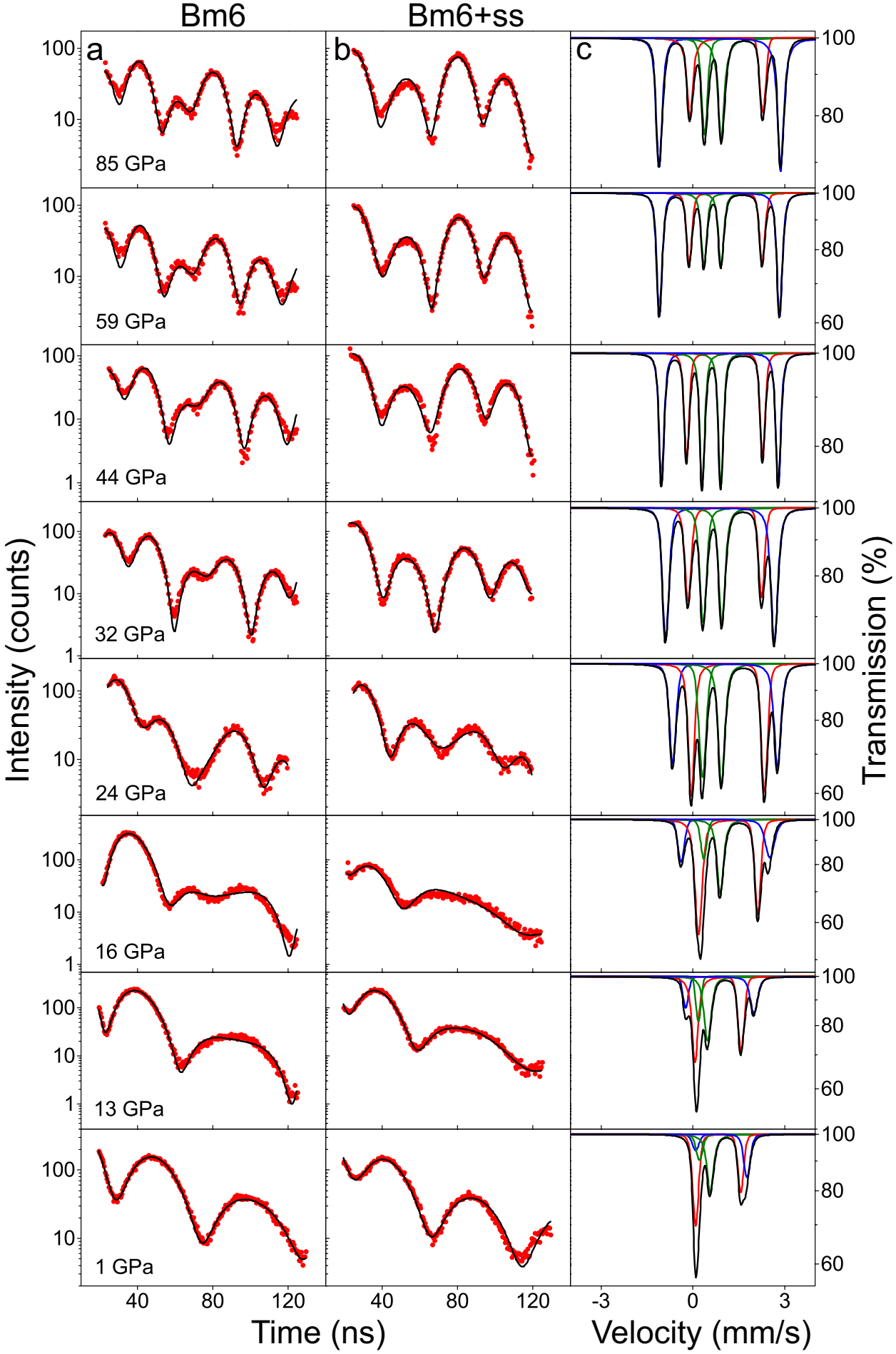
Bm6
Bm6+ss
a
b
c
85 GPa
59 GPa
44 GPa
32 GPa
24 GPa
16 GPa
13 GPa
1 GPa
Intensity (counts)
Transmission (%)
Time (ns)
Velocity (mm/s)
40
80
120
-3
0
3

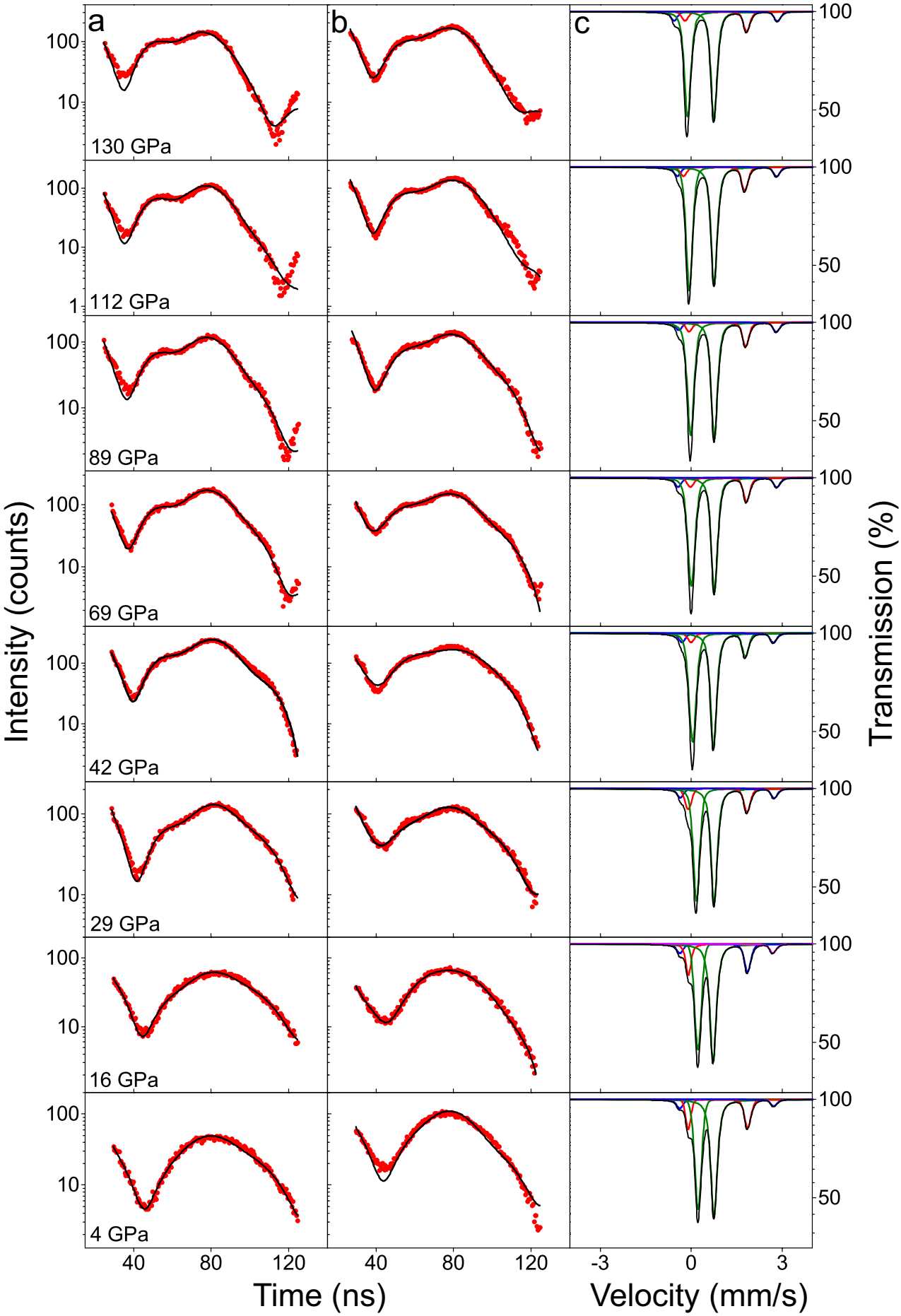
Al-Bm11
Al-Bm11+ss
a
b
c
130 GPa
112 GPa
89 GPa
69 GPa
42 GPa
29 GPa
16 GPa
4 GPa
Intensity (counts)
Transmission (%)
Time (ns)
Velocity (mm/s)
40
80
120
-3
0
3

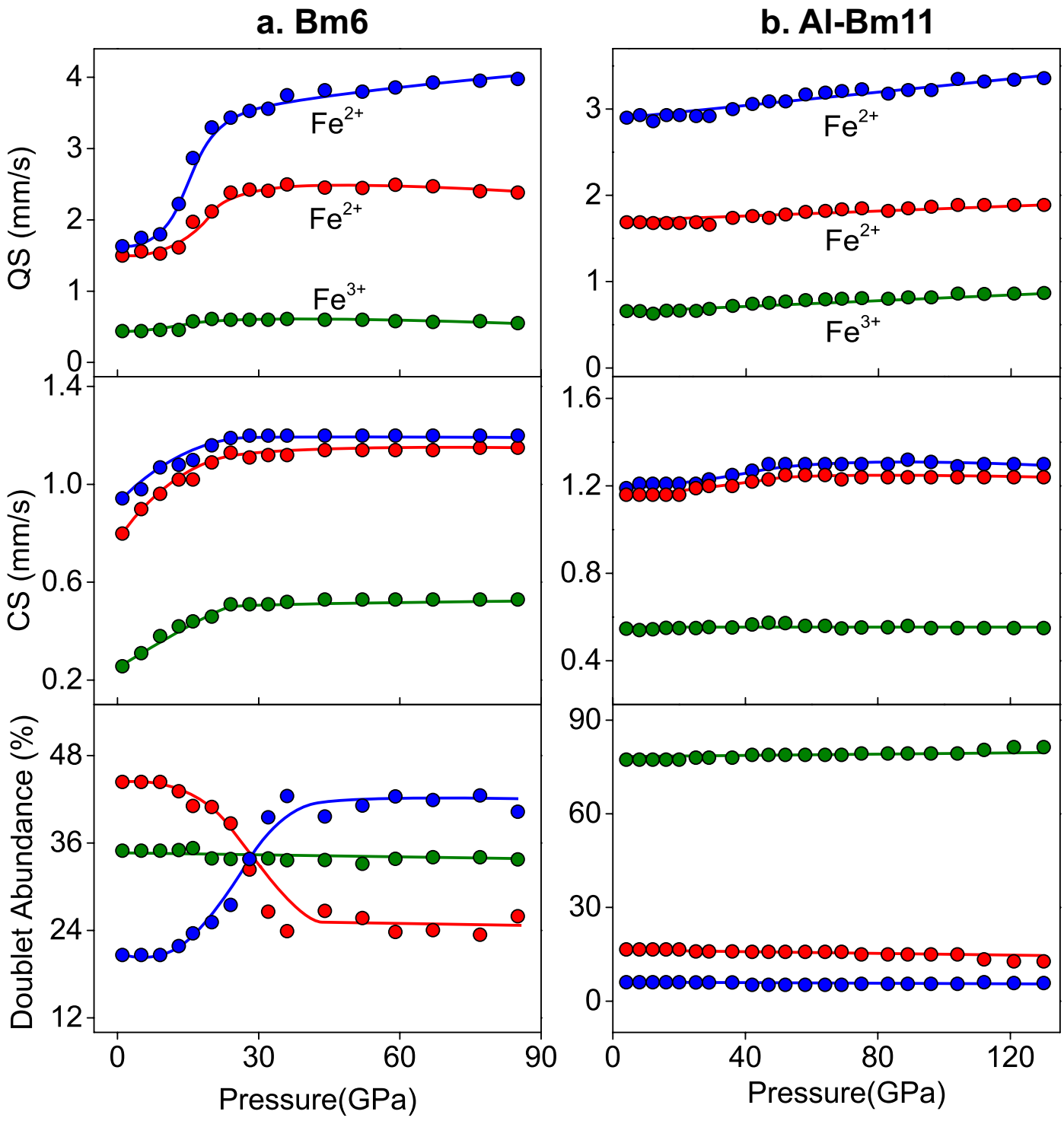
a. Bm6
b. Al-Bm11
QS (mm/s)
CS (mm/s)
Doublet Abundance (%)
Fe2+
Fe2+
Fe3+
Fe2+
Fe2+
Fe3+
Pressure(GPa)
Pressure(GPa)

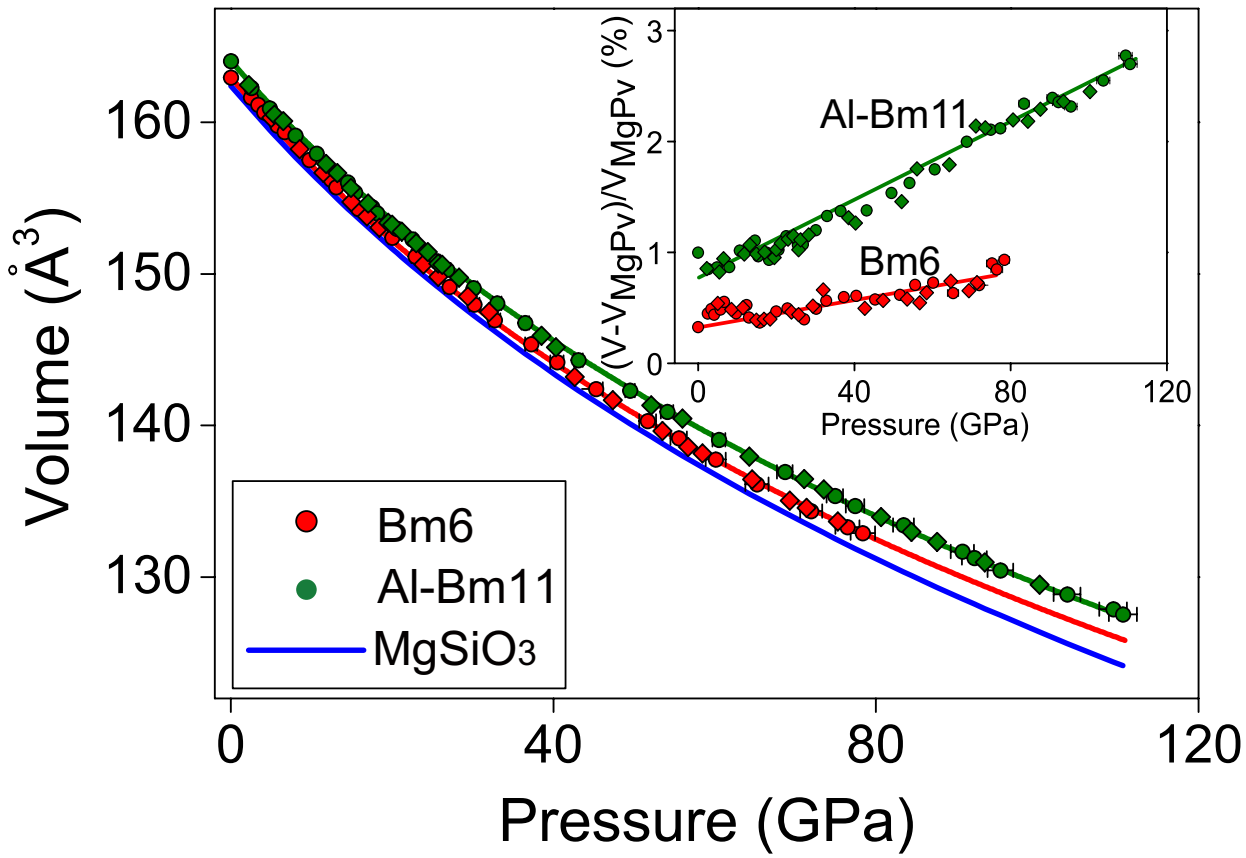
Volume (Å^3)
160
150
140
130
0
40
80
120
Pressure (GPa)
Bm6
Al-Bm11
MgSiO3
(V-V$_{MgPv}$)/V$_{MgPv}$ (%)
3
2
1
0
Al-Bm11
Bm6
0
40
80
120
Pressure (GPa)

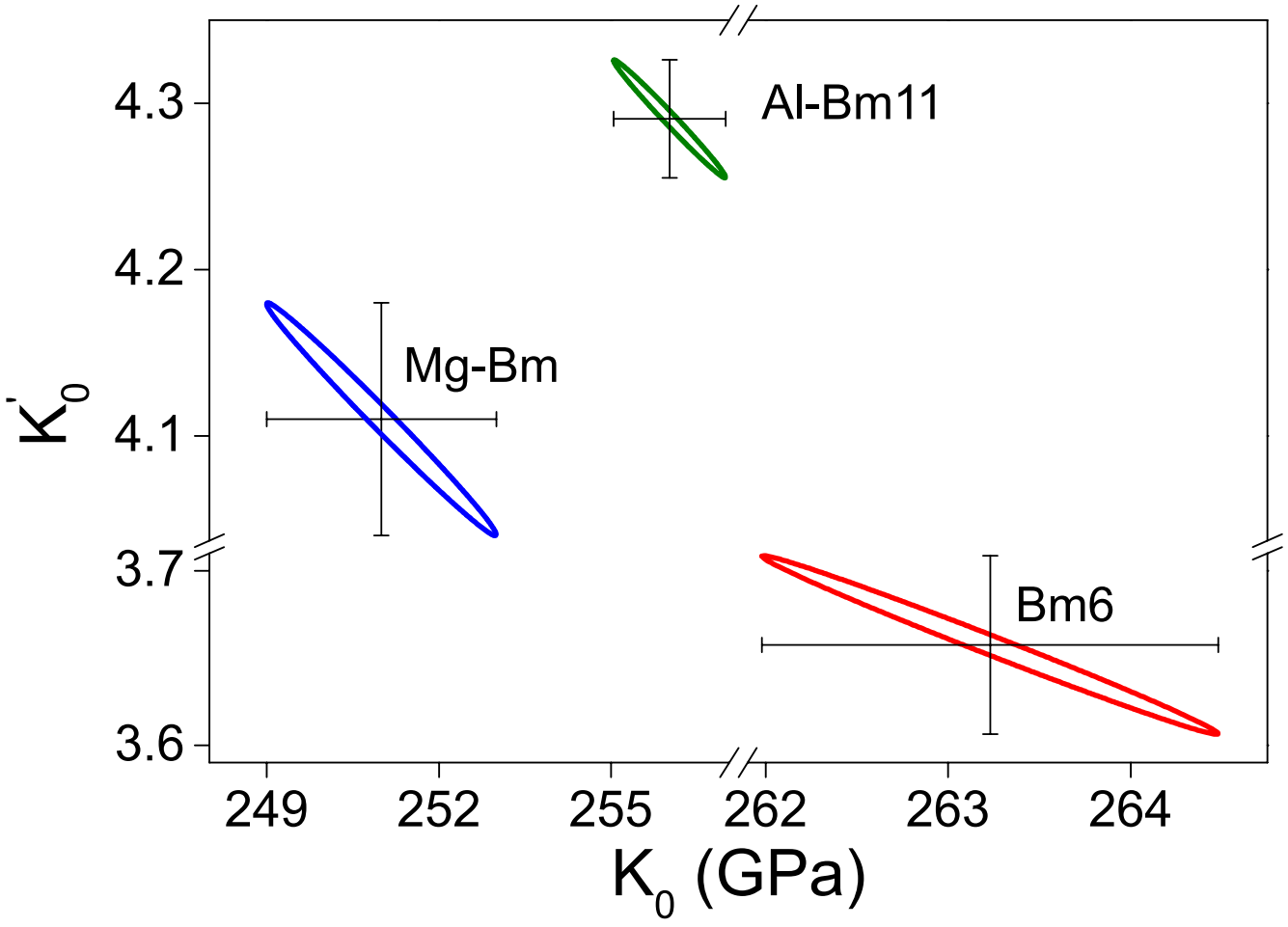
Al-Bm11
Mg-Bm
Bm6
4.3
4.2
4.1
3.7
3.6
K'0
249
252
255
262
263
264
K0 (GPa)

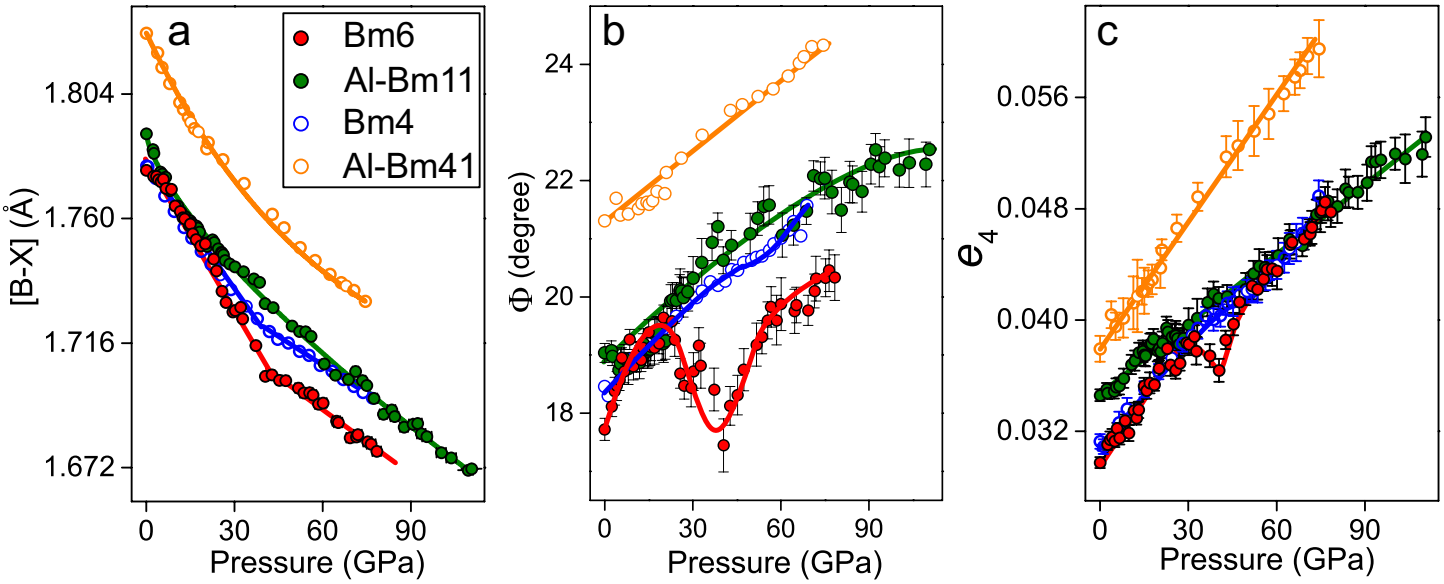
a
Bm6
Al-Bm11
Bm4
Al-Bm41
[B-X] (Å)
1.804
1.760
1.716
1.672
0
30
60
90
Pressure (GPa)
b
Φ (degree)
24
22
20
18
0
30
60
90
Pressure (GPa)
c
e_4
0.056
0.048
0.040
0.032
0
30
60
90
Pressure (GPa)

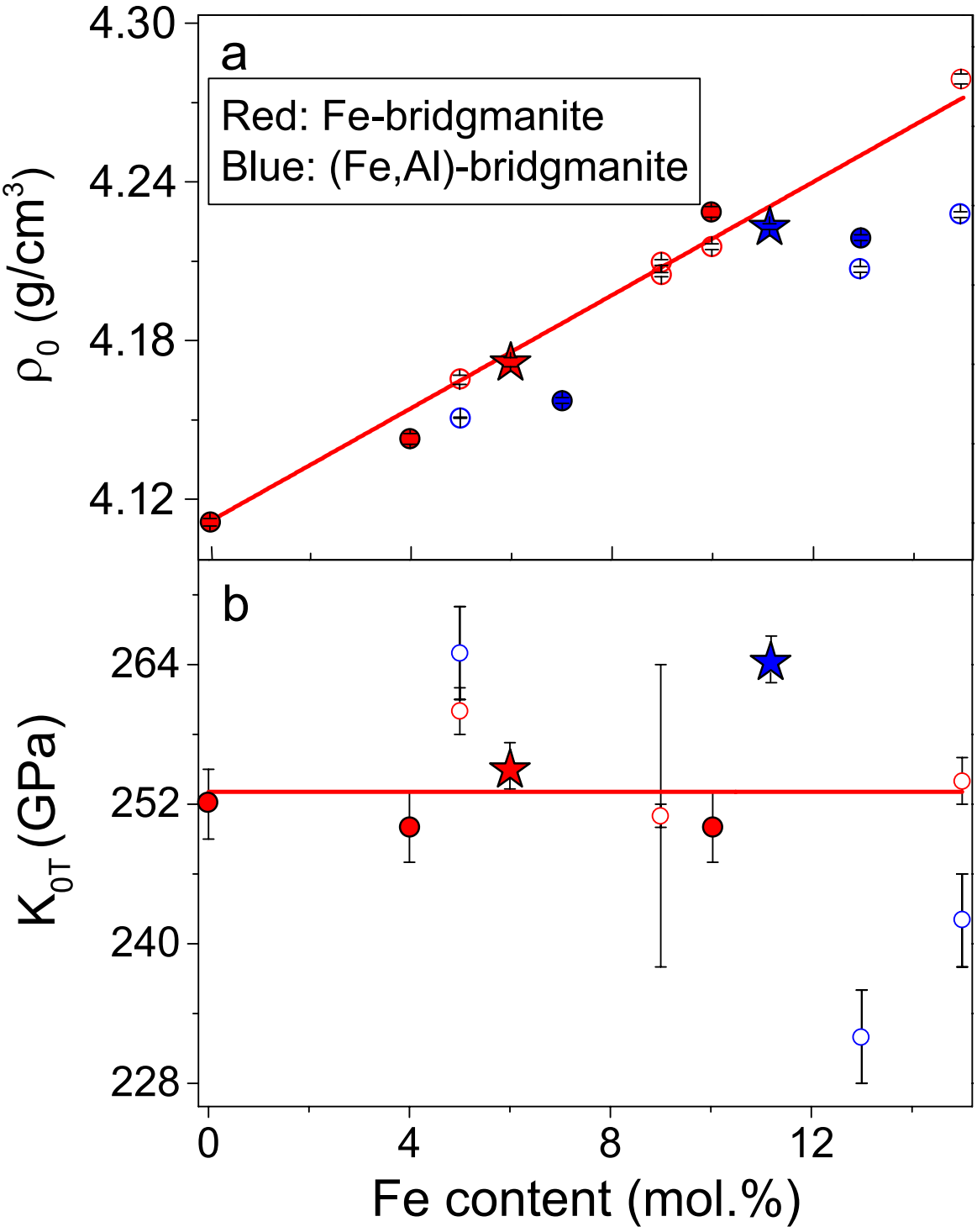
a
Red: Fe-bridgmanite
Blue: (Fe,Al)-bridgmanite
ρ_0 (g/cm^3)
4.30
4.24
4.18
4.12
b
K_{0T} (GPa)
264
252
240
228
0
4
8
12
Fe content (mol.%)

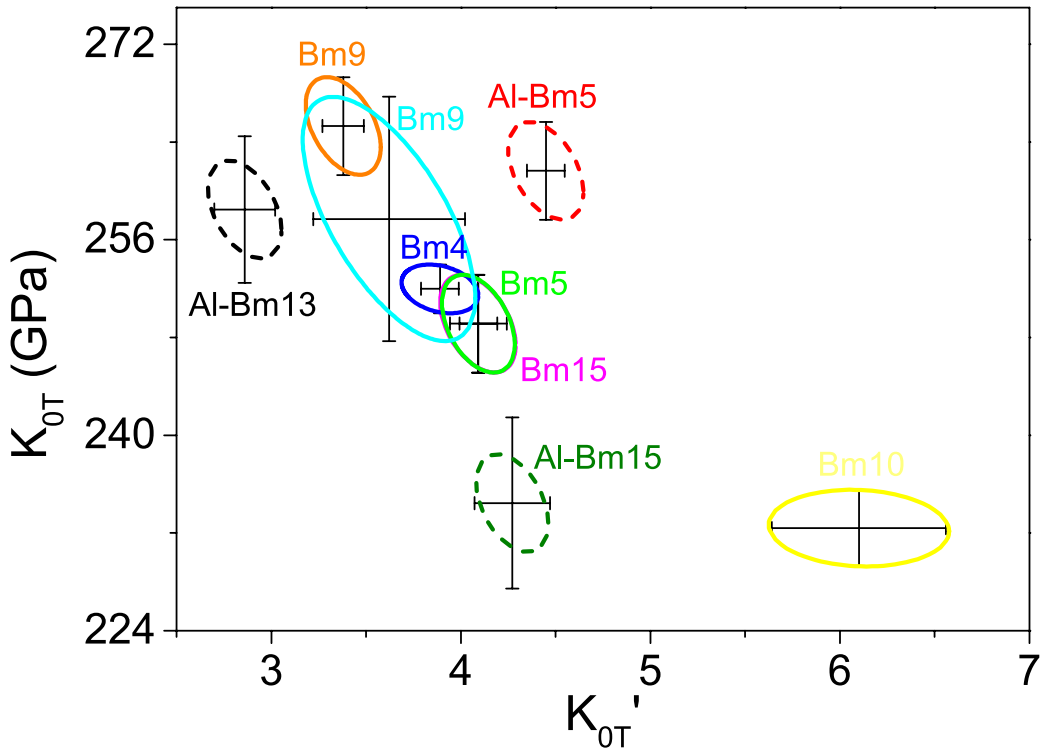
272
256
240
224
3
4
5
6
7
K_{0T} (GPa)
K_{0T}'
Bm9
Bm9
Al-Bm5
Al-Bm13
Bm4
Bm5
Bm15
Al-Bm15
Bm10

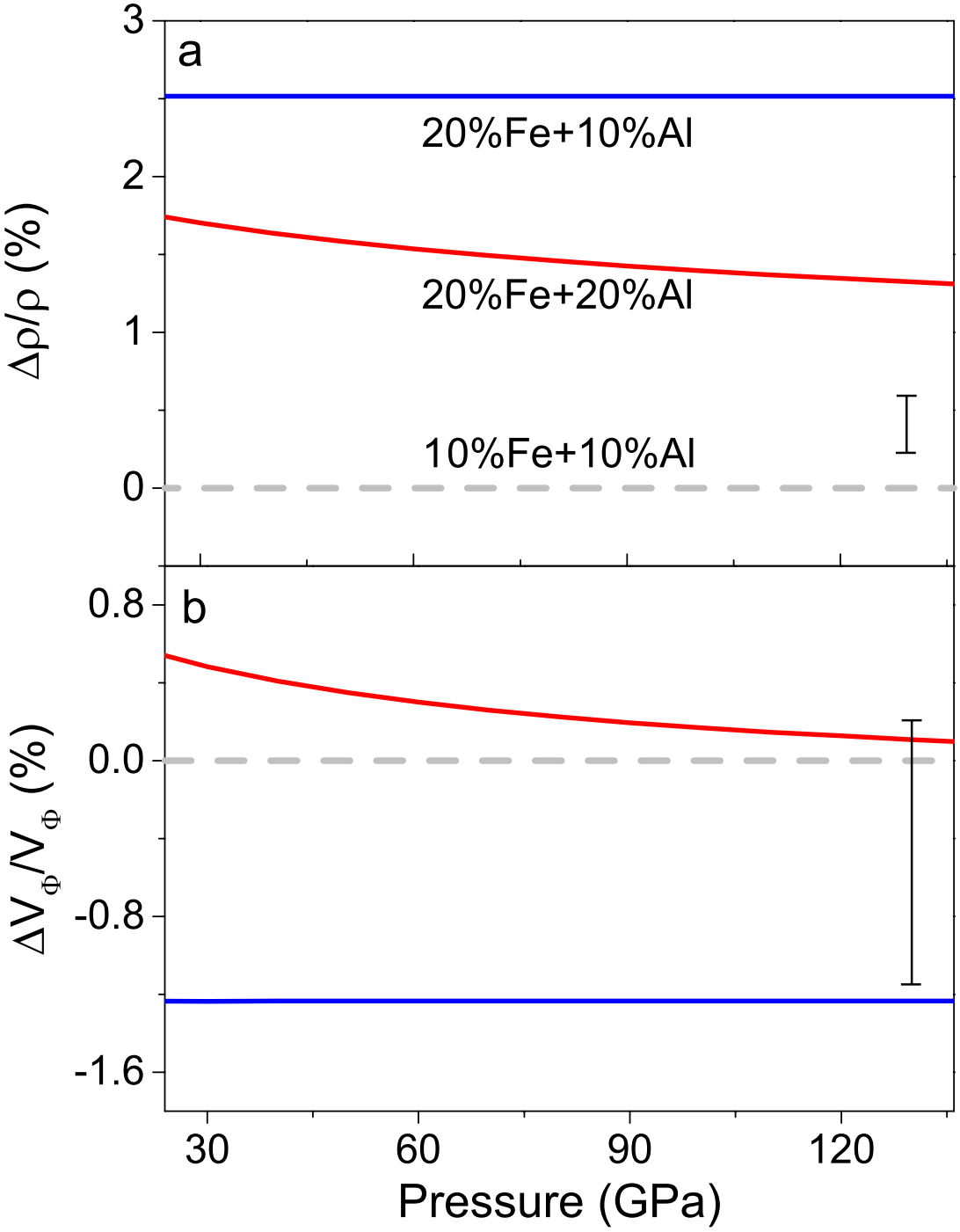
a
20%Fe+10%Al
20%Fe+20%Al
10%Fe+10%Al
Δρ/ρ (%)
3
2
1
0
b
ΔV_Φ/V_Φ (%)
0.8
0.0
-0.8
-1.6
30
60
90
120
Pressure (GPa)